Arctic springtime observations of volatile organic compounds during the OASIS-2009 campaign

Rebecca S. Hornbrook[1], Alan J. Hills[1], Daniel D. Riemer[2], Aroob Abdelhamid[3], Frank M. Flocke[1], Samuel R. Hall[1], L. Gregory Huey[4], David J. Knapp[1], Jin Liao[4,a,b], Roy L. Mauldin III[1,c,d], Denise D. Montzka[1], John J. Orlando[1], Paul B. Shepson[5,6], Barkley Sive[7,e], Ralf M. Staebler[8], David. J. Tanner[4], Chelsea R. Thompson[5,b], Andrew Turnipseed[1], Kirk Ullmann[1], Andrew J. Weinheimer[1], and Eric C. Apel[1]

[1]Atmospheric Chemistry Observations and Modeling Laboratory, National Center for Atmospheric Research, Boulder, Colorado, USA.
[2]Rosenstiel School of Marine and Atmospheric Science, University of Miami, Miami, Florida, USA.
[3]Department of Chemistry and Biochemistry, University of Colorado Boulder, Boulder, CO, USA.
[4]School of Earth and Atmospheric Sciences, Georgia Institute of Technology, Atlanta, Georgia, USA.
[5]Department of Chemistry, Purdue University, West Lafayette, Indiana, USA.
[6]Department Earth, Atmospheric, and Planetary Sciences and Purdue Climate Change Research Center, Purdue University, West Lafayette, Indiana, USA.
[7]University of New Hampshire, Durham, New Hampshire, USA.
[8]Air Quality Processes Section, Environment and Climate Change Canada, Toronto, Canada.
[a]now at: Cooperative Institute for Research in Environmental Sciences, University of Colorado Boulder, Boulder, Colorado, USA.
[b]now at: Chemical Sciences Division, Earth System Research Laboratory, NOAA, Boulder, Colorado, USA.
[c]now at: University of Helsinki, Helsinki, Finland.
[d]now at: Department of Atmospheric Oceanic Sciences, University of Colorado Boulder, Boulder, CO, USA.
[e]now at: Air Resources Division, National Park Service, Lakewood, Colorado, USA.

Corresponding author: Rebecca S. Hornbrook, National Center for Atmospheric Research, P.O. Box 3000, Boulder, CO, 80307, USA (rsh@ucar.edu)

Key Points:

- Integrated Cl and Br atom concentrations calculated from NMHC are decoupled
- Strong positive correlation observed between ozone and aldehyde depletion events
- Alkane - Cl reactions play a key role in OVOC chemical fluxes in the Arctic

This article has been accepted for publication and undergone full peer review but has not been through the copyediting, typesetting, pagination and proofreading process which may lead to differences between this version and the Version of Record. Please cite this article as doi: 10.1002/2015JD024360

Abstract

Gas-phase volatile organic compounds (VOCs) were measured at three vertical levels between 0.6 m and 5.4 m in the Arctic boundary layer in Barrow, Alaska for the Ocean-Atmosphere-Sea Ice-Snowpack (OASIS)-2009 field campaign during March - April 2009. C_4-C_8 nonmethane hydrocarbons (NMHCs) and oxygenated VOCs (OVOCs), including alcohols, aldehydes and ketones, were quantified multiple times per hour, day and night during the campaign using *in situ* fast gas chromatography-mass spectrometry. Three canister samples were also collected daily and subsequently analyzed for C_2-C_5 NMHCs. The NMHCs and aldehydes demonstrated an overall decrease in mixing ratios during the experiment whereas acetone and 2-butanone showed increases. Calculations of time-integrated concentrations of Br atoms, $\int[\mathrm{Br}]dt$, yielded values as high as $(1.34 \pm 0.27) \times 10^{14}$ cm^{-3} s during the longest observed ozone depletion event (ODE) of the campaign, and were correlated with the steady state Br calculated at the site during this time. Both chlorine and bromine chemistry contributed to the large perturbations on the production and losses of VOCs. Notably, acetaldehyde, propanal and butanal mixing ratios dropped below the detection limit of the instrument (3 parts per trillion by volume (pptv) for acetaldehyde and propanal, 2 pptv for butanal) during several ODEs due to Br chemistry. Chemical flux calculations of OVOC production and loss are consistent with localized high Cl-atom concentrations either regionally or within a very shallow surface layer, while the deeper Arctic boundary layer provides a continuous source of precursor alkanes to maintain the OVOC mixing ratios.

Index Terms: 9315 Arctic Region, 0365 Troposphere: composition and chemistry, 0368 Troposphere: constituent transport and chemistry, 3307 Boundary Layer Processes

Keywords: VOCs, hydrocarbons, OVOCs, Arctic chemistry, snow-air exchange, halogen atoms, ozone depletion events

1. Introduction

Since the earliest discovery of rapid ozone depletion events (ODEs) from the Arctic atmospheric boundary layer [*Bottenheim et al.*, 1986; *Oltmans and Komhyr*, 1986], much work has been done to better understand the chemical mechanisms involved and the overall impact on Arctic chemistry [*Barrie et al*., 1988; *Ramacher et al*., 2000; *Simpson et al*., 2007; *Tackett et al*., 2007; *Thompson et al*., 2015; *Toyota et al*, 2014]. Three major oxidants can be present in the Arctic boundary layer: hydroxyl radicals (OH), Cl atoms, and Br atoms. A number of studies have shown that bromine atom chemistry is primarily responsible for the ozone depletion [*Barrie et al*., 1988; *Fan and Jacob*, 1992; *Finlayson-Pitts et al*., 1990; *McConnell et al*., 1992; *Pratt et al*., 2013; *Thompson et al*., 2015], while many nonmethane hydrocarbons (NMHCs) are concurrently depleted by Cl oxidation [*Ariya et al*., 1998; *Boudries and Bottenheim*, 2000; *Jobson et al*., 1994; *Ramacher et al*., 1999; *Rudolph et al*., 1999; *Yokouchi et al*., 1994]. *Jobson et al*. [1994] observed that the decay of specific NMHCs during ODEs could not be explained by OH chemistry alone and took advantage of the fact that alkanes react with chlorine at a significant rate and ethyne reacts with both chlorine and bromine at significant rates to infer the exposure to Cl and Br atoms during the history of an air parcel. From a recent study, it was shown that the release of gas-phase bromine is most efficient from fresh snow over first-year sea ice [*Pratt et al.*, 2013]. The frequency of March ODEs is increasing and correlated with the decline in multiyear ice [*Oltmans et al*., 2012],

which suggests that the impact of halogen chemistry and ODEs on Arctic chemistry may become more pronounced as climate change progresses.

Several studies have used measurements of oxygenated volatile organic compounds (OVOCs) in addition to NMHCs to gain insight into oxidation pathways and their spatial extent occurring in the Arctic. *Guimbaud et al*. [2002] showed that inside an ODE at Alert, Nunavut, during the springtime ALERT2000 field campaign, a substantial loss of propane corresponded to a concomitant increase in acetone. From the same study, *Boudries et al*. [2002] observed that acetone, which ranged between 18-1470 pptv, was the only observed OVOC species that increased in mixing ratio during that time. The authors did not observe a seasonal trend in 2-butanone (methyl ethyl ketone; MEK), which is primarily a product of the oxidation of *n*-butane in the Arctic environment with a smaller contribution from 3-methylpentane oxidation and possibly some long-range transport of MEK to the region in the wintertime. *Tackett et al*. [2007] used the ratio of balloon observations of MEK and *n*-butane from Barrow to assess the impact of chlorine chemistry on a vertical scale. The authors reported that on a day when the ozone was only slightly depleted (i.e., to 27 parts per billion by volume, ppbv), *n*-butane was significantly lower at the surface than at a height of 20 m. At the same time, MEK concentrations were higher at the surface than aloft, leading the authors to conclude that the source of halogens that consumes ozone (O_3) and volatile organic compounds (VOCs) appears to originate from the snowpack, and that the chemistry occurs over a small vertical scale, likely within the first few 10s of meters.

The sunlit snowpack is highly photochemically active [*Galbavy et al*., 2007; *Lee-Taylor and Madronich*, 2002] and has been shown to exchange reactive species with the atmosphere [*Anastasio and Robles*, 2007; *Beine et al*., 2008; *Dominé and Shepson*, 2002]. Snow-air exchange of HCHO has been investigated at a number of high-latitude sites over the Arctic and Antarctic snowpack [*Barret et al*., 2011; *Hutterli et al*., 1999, 2002; *Preunkert et*

al., 2015; *Salmon et al*., 2008; *Sumner and Shepson*, 1999]. In addition to HCHO, several other chemically reactive species such as Br_2 [*Foster et al*., 2001], hydrogen peroxide (H_2O_2), nitrogen oxides (NO_x; NO + NO_2) and nitrous acid (HONO) [*Beine et al*., 2002; *Dibb et al*., 2004; *Honrath et al*., 1999, 2002; *Jacobi et al*., 2002], as well as several other OVOCs have been reported to be emitted from the snowpack. The OVOCs include acetaldehyde and acetone [*Guimbaud et al*., 2002; *Houdier et al*., 2002], and formic and acetic acids [*Dibb and Arsenault*, 2002]. Modeling of the diurnal variations of low-molecular weight carbonyl data indicate a strong dependence on the photochemically-driven emissions and temperature-dependent uptake of the snowpack, an impact that could be tested through measurements in the lowest 100 m of the boundary layer [*Grannas et al*., 2002]. *Grannas et al*. [2007] present an overview of this subject.

This study reports measurements during the months of March and April 2009 from a field site near Barrow, Alaska. A wide range of NMHCs and OVOCs were quantified using continuous diurnal *in situ* fast gas chromatography-mass spectrometry (fast-GC/MS) analyses and daily (2-3 per day) canister collection with subsequent analysis in the laboratory. Together, the two techniques cover C_2-C_8 NMHCs, alcohols, aldehydes and ketones providing to date the most comprehensive Arctic VOC dataset in terms of species measured and temporal coverage. Goals of the study include the following: 1) obtaining high accuracy measurements of all species including the aldehydes for which few measurements exist in the literature; 2) gaining additional knowledge of seasonal VOC behavior driven by OH chemistry; 3) investigating in-depth the relationships between VOCs and halogen atoms before, during, and after low ozone events; and 4) using the VOC measurements in concert with the radical measurements at the site to gain a better understanding of the oxidation pathways occurring in the Arctic.

2. Experimental

2.1 Measurement Site and Sampling

The primary gas-phase and pristine-snow measurement site for the OASIS-2009 field campaign was located approximately 150 m southeast of the Barrow Arctic Research Center, approximately 5.5 km northeast of the town of Barrow, Alaska (71.30°N, 156.77°W). The site included two custom-built instrumented trailers (Module 1 and Module 2) and two measurement towers (6.1-m Tower 1 and 10-m Tower 2), shown in Figure 1 (inset b) and described previously [*Boylan et al*., 2013; *Helmig et al*., 2012; *Liao et al*., 2011; *Villena et al*., 2011]. Non-radical gas-phase measurement instruments, including the National Center for Atmospheric Research (NCAR) Trace Organic Gas Analyzer (TOGA), were housed in Module 1 and sampled from Tower 1.

Ambient air was continuously drawn with Gast diaphragm pumps at flow rates ≥ 19 standard liters per minute (slm) through each of three heated (35 °C) ½-in. O.D. electropolished stainless steel (SS) tubes with inlet heights at approximately 0.6 m, 1.5 m and 5.4 m above the clean snow surface, variable up to approximately ± 0.3 m due to drifting snow at the base of Tower 1. The sampling tower was located approximately 3.5 m north of the NE corner of Module 1. Residence time in the sample lines varied between 1.2 seconds for the 0.6-m tower inlet and 2.3 seconds for the 5.4-m inlet. Each sampling line was tested for NMHC and OVOC transmission efficiency by adding the OASIS calibration standard (see below) to the inlet of each sampling line, and in all cases the retrieved mixing ratio was within 3% of the input values. These sampling lines were shared with the NCAR Difference Frequency Generation Tunable Diode Laser Spectroscopy (DFGAS) instrument making HCHO measurements. The instruments had the capability of sampling from any one of the three heated lines at any time but were generally programmed to sequentially sample at various times as described below.

Sampling line selection was computer-controlled through a sampling manifold using pneumatic 2-way valves. The TOGA system sampled ambient air from the sample lines, prior to the air going through the Gast pumps, at a rate of 5 slm through a ¼-in. electropolished SS tube. Between 7 and 15 March, the TOGA sampling manifold cycled between the three heated lines on Tower 1 twice per hour, sampling at ten-minute intervals from each line. Between 15 March and 4 April, the manifold sampled from the three inlets on Tower 1 during the first half of each hour for ten minutes from each line. Between 4 April and the end of the campaign, the sampling cycle frequency was increased such that the manifold sampled from the three inlets on Tower 1 switching between inlets every five minutes.

2.2 Measurements

2.2.1 The Trace Organic Gas Analyzer (TOGA)

The TOGA was used to quantify mixing ratios of 18 VOCs during the OASIS-2009 field campaign. Integrated samples were obtained for 40 seconds and analyzed at a frequency of one sample every ten minutes for the first four weeks of the campaign beginning on 7 March, and one sample every five minutes from 4 April until the end of the campaign on 13 April. The major components of the TOGA system, described previously by *Apel et al*. [2010], include an electropolished stainless steel (SS) inlet, heated to ensure that the compounds of interest were quantitatively transferred from the inlet to our analytical system, cryogenic pre-concentrator, gas chromatograph (GC), mass spectrometer (MS), and zero air/calibration system. All processes and data acquisition were computer controlled. For the pre-concentrator, all tubing was Silcosteel™ (Restek Corporation, Bellefonte, PA). The water trap was made with 1/8-in. O.D. tubing, the enrichment trap was made of 1/16-in. O.D. tubing, and the cryofocussing trap was made of 0.029-in. O.D. tubing. The cryofocussing trap and water trap were open tubes and the enrichment trap contained glass wool for additional

surface area. For the enrichment cycle, the water trap and enrichment traps were cryogenically cooled using liquid-nitrogen cooled N_2 to -20 °C and -130 °C, respectively. The flow rate during sampling was 40 standard cubic centimeters per minute (sccm) and the sample collection time was 40 seconds, yielding a sample volume of 27 cm^3. Following this, the enrichment trap was heated at 25 °C s^{-1} from -130 °C to 100 °C and trapped VOCs were transferred with He carrier gas at 1 sccm to the cryofocussing trap cooled to -130 °C. The cryofocusing trap was then heated, also at 25 °C s^{-1}, from the cold set-point to 100 °C in the presence of 1 sccm flow of He carrier gas, thereby injecting the sample onto the gas chromatograph (GC).

The GC is a custom-designed unit that is lightweight and temperature programmable, fitted with a Restek MXT-624 column (I.D. = 0.18 mm, film thickness = 1 µm, length = 8 m). Limits of detection (LODs) are compound specific and range from 1 pptv (parts per trillion by volume) to 100 pptv (Table 1). The system was calibrated several times during the field study using a mixture prepared gravimetrically in-house containing 15 of the 18 VOCs (see below for species quantified). The C_8-aromatics *m*-xylene, *p*-xylene and *o*-xylene were not included in the OASIS standard. The calibration mixture containing the VOCs in the 200-500 ppbv mixing ratio range was dynamically diluted using a custom-built catalytic-clean air generator/dynamic dilution system (ZA/CS) [*Apel et al*., 2003; *Guenther and Hills*, 1998]. The dilution system employs two calibrated mass flow controllers for the calibration mix (0-30 sccm) and the diluent gas (0-10 slm). The system was used to dilute the ppbv-level OASIS standard to ambient-level mixing ratios. This arrangement yields accurate (±1%) and precise (±1%) gas delivery. The diluent gas is generated via ambient air scrubbed via catalytic oxidation (platinum on alumina at 425 °C), providing diluent gas at ambient humidity levels and permanent gas mixing ratios of the air masses under investigation.

Before and after the OASIS experiment the TOGA instrument was calibrated in the laboratory with a number of different calibration mixtures, including standards containing the xylenes. NCAR ACOM (formerly ACD, the Atmospheric Chemistry Division) maintains a large set of NMHC and OVOC standards. Some of these have been used in national and international intercomparison experiments that have been run by our laboratory to help ensure that VOC datasets collected by various groups around the world are of high quality and comparable to one another. We have worked closely with the National Institute of Standards and Technology (NIST) to develop a number of different NMHC standards in the ppbv range [*Apel et al*., 1994; 1995; 1999; 2003; *Volz-Thomas et al*., 2002]. We used diluted NIST Standard Reference Material (SRM) standards and NIST ppbv mixtures prepared specifically for our laboratory to calibrate TOGA before and after the experiment [*Apel et al*., 2015]. We also referenced the NMHCs in our in-house prepared OASIS calibration mixture with the NIST standards. For the three compounds that were missing from our OASIS calibrated mixture, *m*-,*p*-, and *o*-xylene, we used a NIST 19-component standard specially prepared for our laboratory for the *o*-xylene calibration and in-house prepared mixtures of *m*-xylene and *p*-xylene that were cross-referenced to prepared mixtures from Scott-Marrin, Inc. and Environment Canada. The OVOCs were calibrated with our in-house standards. Our group has extensive experience in preparing these standards [*Apel et al*., 1998a; 1998b] and in cross-comparing with other prepared mixtures from Scott-Marrin, Inc. and Scott Specialty Gases. OVOC standards prepared by our group have been used throughout the world for OVOC calibrations. We are also familiar with OVOC measurement challenges and techniques required for their successful measurement [*Apel et al*., 2008]. Although ozone artifacts are believed to complicate measurements of carbonyl compounds, and in particular measurements of aldehydes, we know that ozone artifacts on TOGA observations are

minimal based on ozone interference tests performed on TOGA systems. These tests are described in Text S1 in the supporting information.

The VOCs quantified by TOGA during OASIS-2009 include NMHC (C_4 and C_5 alkanes, benzene, toluene, C_8-aromatic hydrocarbons) and OVOCs (acetaldehyde (CH_3CHO), propanal (C_2H_5CHO), butanal (C_3H_7CHO), methanol (CH_3OH), ethanol (C_2H_5OH), acetone (CH_3COCH_3), methyl ethyl ketone (MEK; $C_2H_5COCH_3$), and 2-pentanone ($CH_3COC_3H_7$)). The data range (minimum and maximum mixing ratios), mean and standard deviations for the TOGA-observed VOCs are summarized in Table 1. For TOGA data with minimum mixing ratios below detection limit (bdl), the mean and standard deviation are calculated using non-zero approximations for bdl data equal to the number of data points above the detection limit N (included in Table 1) divided by the total number of samples × the LOD for that VOC. I.e., for a VOC with 25% of samples below a detection limit 2 pptv, the data below the detection limit are replaced with 1.5 pptv for these statistics. For some VOCs, e.g., benzene and ethanol, the number of samples N is less than the total number of TOGA samples due to temporary chromatographic shifts, and not because the mixing ratios were bdl.

2.2.2 Canister samples

Whole air samples were collected in 2-L electropolished SS canisters at a frequency of approximately three per day, generally one each during the morning, midday and afternoon. The canisters were collected through the 5.4-m heated SS line on Tower 1. Sampling involved pulling air through the heated line into the SS canisters and pressurizing to 35 psig with a metal bellows pump (Senior Flexonics, MB 602). The canisters were shipped and subsequently analyzed at the University of New Hampshire by gas chromatography (GC) with flame ionization, electron capture, and mass spectrometric detection no later than two months after the end of the field campaign [e.g., Russo et al., 2010a, 2010b; Swarthout et al., 2013; Zhou et al., 2008]. The GC analysis included trace

gases comprising selected C_2-C_5 NMHCs including ethane, ethyne, propane, *n*-butane, isobutane, *n*-pentane and isopentane (Table 2). To ensure traceability to international NMHC standards, whole air and synthetic standards were routinely analyzed and calibration scales were cross referenced and validated. When conducting the canister sample analysis for this work, one of two whole air standards was analyzed after every eighth sample in order to monitor the detector sensitivity and measurement precision, and finally spurious data points were removed upon careful re-examination of the full data set. Details regarding calibrations and standard analysis can be found in Sive et al. [2005], Russo et al. [2010b] and Swarthout et al. [2013].

2.2.3 Meteorological and turbulence data

Meteorological data were obtained by several groups during the study, either at the field site or nearby. Participants from NCAR measured wind direction and wind speeds at 5.4 m agl on Tower 1 (Figure 1). NCAR meteorological data were obtained between 7 March and 8 April at 10:00 local time (AKST; Alaskan Standard Time). Environment Canada (EC) participants reported several meteorological parameters from Tower 2 (see Figure 1, inset b), including temperature and relative humidity at 2 m agl, wind direction at 3 m agl pointing towards 60° true, and wind speed at 10 m agl. EC meteorological data were obtained between 8 March and 6 April at 14:00 AKST. Finally, wind directions and wind speeds observed at the NOAA Barrow Observatory approximately 1 km NE of the sampling site (Figure 1, inset a) were available for the majority of the field study between 7 March and 14 April.

The 1-min average wind speeds and 1-min average wind directions were determined using the averaged data from all three wind measurement locations, i.e., Tower 1, Tower 2 and the NOAA Barrow Observatory. The reported NCAR wind directions were, on average, 20° greater than the other two measured wind directions, and so the NCAR wind directions were corrected by -20° for consistency. 1-min average wind directions are the mean of the

three wind direction measurements (NOAA, NCAR-corrected and EC), or of whichever measurements were available. Likewise, 1-min average wind speeds were determined as the mean of the three wind speed measurements, or of whichever measurements were available. Hereinafter, we refer to 1-min average wind speeds and 1-min average wind directions as wind speeds and wind directions, respectively.

2.2.4 Other Measurements

O_3 and nitric oxide (NO) were measured on NCAR Tower 1 with an NCAR-built chemiluminescence (CL) instrument [*Ridley and Grahek*, 1990; *Ridley et al.*, 1992], also housed in Module 1. A sample flow of 3.5 L min^{-1} was directed to the CL from a primary manifold sampling 10-min sequential periods at 5.8 L min^{-1} through three ¼-in. O.D. PTFE tubes connected to three additional heated inlets at 0.6 m, 1.8 m and 5.4 m on Tower 1. Hourly *in situ* ozone mixing ratios were also measured at the NOAA Barrow Observatory [*McClure-Begley et al*., 2014]. For this work, ozone observations from both the NCAR CL and the NOAA Observatory were merged into a 1-minute average O_3 data set such that the 1-min NCAR O_3 data are used where they exist, then a 20-min running average of the NCAR O_3 is used where it exists, then a 60-min running average of the NCAR O_3 is used where it exists, and where no NCAR O_3 data are available for > 60 min, the NOAA O_3 data are used. Between 7 March and 14 April, there were a total of 3.9 days during which no NCAR ozone measurements were available for > 60 min. Thus, the use of NOAA O_3 data is relatively minimal, and occurred primarily at the beginning of the study before the NCAR CL instrument was operational.

Hydroxyl radicals (OH) were measured every 30 seconds at a height of 1.5 m agl using a chemical ionization mass spectrometer (CIMS) [*Mauldin et al*., 1999] housed inside Module 2, with the inlet aiming southeast, orthogonal to the prevailing winds to minimize wall effects by the exterior wall of the Module. A charged-coupled device Actinic Flux Spectroradiometer (CAFS) [*Shetter and Muller*, 1999] measured spectrally resolved downwelling actinic flux at 0.1 Hz. The upwelling flux was estimated as a function of solar zenith angle using the Tropospheric Ultraviolet and Visible (TUV) radiative transfer model [*Madronich and Flocke*, 1999] under clear sky conditions. The sum of up- and downwelling actinic fluxes was used to calculate total photolysis frequencies.

3. Results and discussion

3.1 Clean-air sector

Based on the orientation of the field site, the clean-air sector for data sampled from Tower 1 is considered to be data collected when the winds originated from 10°-110° with wind speeds > 1 m s^{-1}, comprising 61.8% of the sampling time. Times with wind speeds less than 1 m s^{-1}, considered to be "calm", comprised 3.8% of the sampling period and are not included in the clean-sector data as local sources may have impacted the observations. As a further precaution, to avoid inclusion of air from the direction of the clean sector impacted by local vehicular traffic, samples with toluene mixing ratios exceeding 200 pptv, or demonstrating a significant increase (> 100 pptv) above the previous observations as well as samples taken at times when NO > 200 pptv were eliminated from the clean-sector data. Data that meet the above criteria are considered to be clean-sector data, and are used in the remainder of this work. Overall, from the 3175 TOGA samples taken from Tower 1 during the study, 2106 are included in the clean-sector data, and from the 92 canisters sampled, 54

are included in the clean-sector data. Statistics (data range, mean, standard deviation) for the clean-sector data are summarized in Tables 1 and 2.

Figure 2a shows a time-series plot of the wind directions, colored by the wind speed. Figure 2b shows the daily maximum and daily minimum temperatures. Also included on Figure 2a and 2b are the 1-min O_3 data from the study, as described above. Several partial and near-complete ODEs occurred during the study, four of which occurred when the winds primarily originated from the clean sector. These four events are shaded and labeled in Figure 2a, and are referred to in this work as ODE 1 through ODE 4, and correspond to ODEs 1, 3, 4 and 7 in *Helmig et al*. [2012].

3.2 Comparisons of NMHC measurements

Four alkanes were co-measured by TOGA and from the whole air canisters: *n*-butane, isobutane, *n*-pentane and isopentane. To compare the measurements, a 10-minute merged data file was generated from all clean-sector data such that TOGA and canister samples taken within the same 10-minute time period are compared. Figure S2 shows these comparison plots for the TOGA vs. Canister NMHC measurements. For each comparison plot in Figure S2, an orthogonal distance regression (ODR) is shown, as well as the r^2 value for the linear least-squares regression. All four comparisons indicate good agreement between the canister and the TOGA measurements, with ODR slopes (r^2 values) 1.04 ± 0.02 (0.986), 0.96 ± 0.02 (0.986), 1.04 ± 0.03 (0.978) and 1.03 ± 0.05 (0.922) for the *n*-butane, *n*-pentane, isobutane and isopentane comparisons, respectively.

3.3 NMHC Observations

Figures 3-5 show full study time series of clean-sector NMHC data that are discussed throughout the paper. Figure 3 shows the canister measurements of ethane, ethyne and propane, colored by measured ozone mixing ratios. Mixing ratios of ethane and propane decreased throughout the measurement period. We know from annual polar observations that seasonal trends in NMHC tend to be sinusoidal [*Gautrois et al*., 2003; *Helmig et al*., 2014; *Kramer et al*., 2015; *Swanson et al.*, 2003; *Worton et al*., 2012], but during this limited spring study, the overall trends can be described sufficiently using a linear fit. The observed trends in all alkanes are consistent with previous observations of the seasonality of saturated NMHC in the Arctic during spring, primarily due to increasing OH radical oxidation throughout the spring and summer. An overall decrease in mixing ratios with time was also observed for ethyne, although the observed ethyne is also correlated with ozone (r^2 = 0.751) as both are impacted by Br atom chemistry (at 248 K $k_{Br+ethyne} = 3.74 \times 10^{-14}$ cm^3 molecule^{-1} s^{-1}; Table 3). The trend in the non-depleted ethyne is consistent with the seasonal trends in the above references, the majority of which report observations on the Greenland ice sheet, with little impact from coastal halogen chemistry, while the study from Alert [*Gautrois et al*., 2003] selectively involved samples outside of ODEs.

Figure 4 shows measurements from TOGA and the canisters for the butanes and pentanes, with TOGA data points colored by the measured ozone mixing ratios. Mixing ratios of C_4-C_5 NMHC were observed above the detection limit (3 pptv) during the entire campaign for both the canisters and TOGA. Similar to the C_2-C_3 alkanes, isobutane, *n*-butane, isopentane and *n*-pentane mixing ratios decreased overall during the campaign, consistent with literature seasonal cycles described above (Figure 4; Table 1). Isobutane and *n*-butane mixing ratios were strongly correlated, both in the TOGA observations (r^2 = 0.993, ODR fit slope = 0.550 ± 0.001) and the canisters (r^2 = 0.989, ODR fit slope = 0.5551 ± 0.008) as

shown in Table 4. Likewise, isopentane and *n*-pentane mixing ratios were strongly correlated, both in the TOGA data (r^2 = 0.975, ODR fit slope = 1.073 ± 0.003) and in the canisters with the omission of a single data point in the latter from 19 March at 15:00 AKST (r^2 = 0.965, ODR fit slope = 1.01 ± 0.03; Table 4). Both the TOGA and canister data from that time observed a high *n*-pentane mixing ratio compared to the other alkanes (see Figure 4), suggesting that a very different emission source was briefly impacting the observations. Figure 5 shows time series of the benzene and toluene observations colored by the ozone mixing ratio. Both VOCs were observed at mixing ratios above their respective detection limits for the entire campaign (Table 1). In the TOGA analysis, ethylbenzene, *m*-xylene and *p*-xylene are chromatographically overlapped, and are thus reported as a sum, while *o*-xylene is reported separately. We report statistics on the sum of ethylbenzene, *m*-xylene and *p*-xylene (EMPX), *o*-xylene and the sum of C_8-aromatics in Table 1, which includes *o*-xylene when it is above the detection limit (1 pptv), and a non-zero approximation for data bdl as described above. Clean-sector benzene mixing ratios were observed between 37 and 196 pptv, and toluene mixing ratios between 5 and 114 pptv (Figure 5; Table 1). The clean-sector benzene and toluene mixing ratios are lower than previous measurements made at the NOAA Observatory in Barrow [*Doskey and Gaffney*, 1992], some of which were noted to be impacted by the town of Barrow or Prudhoe Bay: (mean ± standard deviation) 340 ± 80 pptv for benzene and 80 ± 40 pptv for toluene. The lower benzene mixing ratios observed in 2009 are consistent with the EPA findings that show a 45% decrease in benzene at 137 air quality monitoring sites in the United States between 2003 and 2013 [U.S. EPA, 2014a] and also with reductions in benzene emissions between 1990 and 2011 [U.S. EPA, 2014b]. Benzene, toluene, ethylbenzene and xylenes (BTEX) mixing ratios have been shown to be impacted by local sources in otherwise very clean Arctic environments [*Reinmann et al*., 2009], but the

large differences between the statistics on the full data set and the clean-sector data for BTEX (Table 1) suggest that our strategy for eliminating local sources is reasonable.

Correlations between observations of several VOC pairs from both the TOGA and canister data were analyzed, and the results are summarized in Table 4. Where the coefficient of determination of the linear least-squares fit of VOC A vs. VOC B, r^2, is greater than 0.15, linear least-squares and ODR fit parameters are included in the table. The alkanes observed by TOGA and the canisters are all very well correlated, with most individual pairs of alkanes having r^2 values > 0.95. Ethane and propane, with longer atmospheric lifetimes, are slightly less correlated with an r^2 value of 0.858. The aromatic compounds, with more variable emissions and OH reactivities, are less correlated than the alkanes.

During the first week of the study, the observed alkanes varied considerably over relatively short time periods even for the clean-sector data. Strong emissions of highly correlated light alkanes are indicative of oil and natural gas (O&NG) extraction operations. HYSPLIT (HYbrid Single Particle Lagrangian Integrated Trajectory Model) [*Draxler et al*., 2015; *Rolph*, 2015] back trajectories for this time period (available at http://www.oasishome.net/docs/OASIS_HYSPLIT_Back_Trajectories.zip) show air coming from the Beaufort Sea and passing in proximity (often close proximity) to Prudhoe Bay. Prudhoe Bay has the largest oil field in North America in terms of both extraction area and oil production and has been shown to have an impact on gas-phase measurements in Barrow [*Doskey and Gaffney*, 1992; *Jaffe et al*., 1991]. Several natural gas extraction operations exist in the North Slope Borough within 15 km of the OASIS-2009 measurement site (Figure 1), both to the south (South Barrow Gas Pool) and southeast (East Barrow Gas Pool), but since air masses originating from these directions are not included in the clean-air sector, we do not expect to see emissions from these operations in the clean-sector data.

Nevertheless, considering these regional sources, it is likely that we sampled relatively unprocessed O&NG emissions during the first week of the campaign. Adding support to this, Figure 6 shows time-series plots of the isobutane/*n*-butane (iC_4/C_4) and isopentane/*n*-pentane (iC_5/C_5) ratios. Generally, iC_5/C_5 ratios between 1.5 and 2.5 are indicative of urban and vehicular emissions, while iC_5/C_5 ratios close to 1.0 are indicators of recent O&NG extraction emissions [*Gilman et al*., 2013; *Swarthout et al*., 2013; 2015]. In April 2008, as part of the Arctic Research of the Composition of the Troposphere from Aircraft and Satellites (ARCTAS) airborne field campaign on board the NASA DC-8 aircraft, our group made measurements using the TOGA [*Hornbrook et al*., 2011] in the Arctic boundary layer near both Prudhoe Bay and Barrow during which several measurements with strongly enhanced alkane mixing ratios were sampled over both locations. From these data, the iC_4/C_4 ± standard deviation (maximum *n*-butane) observed near Prudhoe Bay and Barrow were 0.47 ± 0.01 (2000 pptv) and 0.59 ± 0.03 (300 pptv), respectively. Likewise, the iC_5/C_5 ± standard deviation (maximum *n*-pentane) were 0.89 ± 0.02 (400 pptv) and 1.3 ± 0.3 (23 pptv) from Prudhoe Bay and Barrow, respectively. (ARCTAS data are publicly available at http://www-air.larc.nasa.gov/missions/arctas/arctas.html.) Although absolute emission ratios vary somewhat between petroleum plays, the mixing ratios of butanes and pentanes and the ratios of the butanes and pentanes observed in Barrow during OASIS-2009, particularly during the first week of the study, point to a recent O&NG extraction emission source.

Finally, there is a general good correspondence of the TOGA data with the canister data, showing that our sampling frequency of three cans per day yielded useful and complementary results.

3.4 NMHCs as indicators for halogen chemistry

The primary oxidants of VOCs in the springtime Arctic environment include OH radicals, Cl atoms and Br atoms. *Jobson et al*. [1994] took advantage of the differing reactivities of NMHCs with OH, Cl and Br in the Arctic (Table 3) to determine the relative impact of the different oxidants. Note that the rate coefficients listed in Table 3 are for reactions at 248 K, the average temperature during the study (Figure 2b). For example, *n*-butane and isobutane have similar rate coefficients with OH, and thus the relative amounts of *n*-butane and isobutane are not expected to change significantly in air masses that experience solely OH oxidation, assuming the emission ratio of iC_4/C_4 is constant. However, Cl atoms react with *n*-butane at a rate 1.5 times faster than Cl atoms with isobutane, so the impact of Cl-atom chemistry would result in higher iC_4/C_4 ratios.

In Figure 6, the iC_4/C_4 ratio 0.55 is shown to indicate the emission ratio from the "freshest" observed emissions from O&NG sources, which we assume to have little or no chlorine processing. There is a clear dependence of the butane ratio on the absolute mixing ratio of *n*-butane, as shown by the color-coded mixing ratios in Figure 6: as observed *n*-butane mixing ratio decreased, iC_4/C_4 increased. As we know from Figure 4 (and Figure 6), both *n*-butane and isobutane decrease with time over the period of the study due to increased photochemistry. However, there is no *a priori* reason to assume that the emission ratio of isobutane to *n*-butane changes. Thus, when we observe changes in the iC_4/C_4 ratio, it can tell us something about the photochemical processing of the two species. Only very modest changes in the ratio can occur due to OH photochemical processing because the OH rate constants are very similar (at 248 K $k_{OH+isobutane} = 1.71 \times 10^{-12}$ and $k_{OH+n\text{-butane}} = 1.72 \times 10^{-12}$, both cm^3 $molecule^{-1}$ s^{-1}; Table 3). The lifetime with respect to OH for the butanes in the Arctic is approximately three weeks for [OH] = 3.2×10^5 molecules cm^{-3} (the average observed OH mixing ratio during first week of the study), and two weeks for [OH] = 4.5 ×

10^5 molecules cm^{-3} (the average mixing ratio during the last week of the study). During this lifetime, the ratio of iC_4/C_4 can only change from 0.55 (assuming the emission ratio from data with no chlorine influence) to 0.56 due to OH processing. To our knowledge, the only emission sources with an iC_4/C_4 emission ratio greater than 0.60 are pure natural gas extraction operations from select plays. Therefore, in the absence of emissions from this type of activity, any ratio greater than ≈ 0.60 must be due to Cl-atom processing. From Figure 6 it is clear that this ratio was generally greater than 0.6 during the study and that the ratio was often near or above 0.8 towards the end of the experiment and during partial or total ODEs. This implies that there was more active Cl chemistry as the study progressed which is consistent (more UV radiation as spring progresses) with the findings of *Liao et al*. [2014], who showed that light and ozone were necessary for Cl_2 (and by implication Cl atoms) to be present. Although chlorine and bromine atoms were not measured directly at the site, steady state $[Cl]_{ss}$ were determined from the measurements that were available [*Liao et al*, 2014; *Stephens et al*., 2012]. Typical midday $[Cl]_{ss}$ was 2×10^5 atoms cm^{-3} and the average $[Cl]_{ss}$ over the period 17 - 29 March was 3.4×10^4 atoms cm^{-3}. A ratio of iC_4/C_4 approaching 0.8 can be achieved by atmospheric processing for seven hours if $[Cl] = 2.0 \times 10^5$ atoms cm^{-3}, or for two days at $[Cl] = 3.4 \times 10^4$ atoms cm^{-3}. These data strongly imply a significant exposure to Cl atoms. It should be noted that measurements at the site do not necessarily reflect the actual exposure that the molecules encountered along their trajectory to Barrow from the northeast. This is discussed in more detail below.

Figure 6 also includes the observed ethyne mixing ratios from the canister measurements. As shown by the rate constants in Table 3, ethyne reacts not only with OH radicals and Cl atoms, but also with Br atoms. In normal background air, the impact of Br atom chemistry on ethyne is small, but in regions where Br atom concentrations are elevated, the loss of ethyne due to Br chemistry can be significant.

Due to differing reaction rates with halogen atoms, the ratios of alkane (RH) mixing ratios in non-halogen-impacted air ($[RH]_{bkg}$) and in halogen-impacted air ($[RH]_{obs}$) can be used to determine the time-integrated Cl-atom concentration $\int[Cl]dt$ [*Jobson et al*., 1994], which gives insight into the oxidation history of an air mass, according to:

$$[RH]_{obs} = [RH]_{bkg} \exp(-k_{Cl}\int[Cl]dt), \quad (1)$$

where k_{Cl} is the rate coefficient for the reaction of Cl atoms with RH. Likewise, similar ratios of ethyne in background air masses and air impacted by bromine chemistry can be used to determine $\int[Br]dt$ using:

$$-k_{Br}\int[Br]dt = \ln([C_2H_2]_{obs}/[C_2H_2]_{bkg}) - \ln([C_2H_2]_{obs}/[C_2H_2]_{bkg})_{Cl}, \quad (2)$$

where k_{Br} is the rate coefficient of Br atoms with ethyne (Table 3).

As noted above, average observed NMHC mixing ratios decreased steadily during the study (e.g., *n*-butane mixing ratios in Figure 4). Thus, rather than assigning a single background mixing ratio (i.e., clean, halogen-chemistry free) to each NMHC for the entire study, time-dependent background VOC mixing ratios, $[RH]_{bkg,t}$, were estimated for TOGA C_4 and C_5 alkanes and canister C_2-C_5 alkanes using the assumption that air masses with iC_4/C_4 ratios less than 0.65 are less likely to be influenced by halogen chemistry. Using a ratio limit lower than 0.65 leaves too few data points for a good fit. Figure 7 shows time-series plots of the observed TOGA mixing ratios as well as daily averages of observed TOGA mixing ratios for all clean-sector data corresponding to iC_4/C_4 ratios of 0.65 of less. Linear fits to the daily averages for each alkane are included on the plots in Figure 7, and are used in the following calculations using TOGA data to estimate $[RH]_{bkg}$ values.

In a similar manner, time-dependent background hydrocarbon mixing ratios, $[RH]_{bkg,t}$, were estimated for the canister ethane, propane, *n*-butane, isobutane, *n*-pentane, and isopentane data. For these data, linear least-squares fits to the daily averages of canister alkanes were calculated, for data where $iC_4/C_4 < 0.65$ (Figure S3). Because ethyne reacts rapidly with Br atoms, which are not always concomitant with active Cl chemistry, background ethyne mixing ratios were estimated using a slightly different methodology. Background time-dependent ethyne mixing ratios, $[C_2H_2]_{bkg,t}$, were determined from a linear least-squares fit to the daily average C_2H_2 mixing ratios where $O_3 > 25$ ppbv (Figure 8), as Br atom chemistry is minimal when O_3 is not depleted [*Thompson et al.*, 2012].

Based on Eq. (1), for each TOGA observation, the slope of a linear fit to a plot of $\ln([RH]_{obs}/[RH]_{bkg})$ against k_{Cl} for each C_4 and C_5 NMHC (Table 3), is equal to $-\int[Cl]dt$. Likewise for each canister measurement, $\int[Cl]dt$ was determined from the slope of a linear fit to $\ln([RH]_{obs}/[RH]_{bkg})$ against k_{Cl} (e.g., Figure 9 shows data sampled on 27 March between 08:56 and 09:00 AKST). The observed ethyne mixing ratios, together with the $\int[Cl]dt$ values determined using the canister data, were used to determine a value for $\int[Br]dt$ for each canister measurement based on Eq. (2).

Figure 10 shows a time-series plot of all the TOGA- and canister-derived $\int[Cl]dt$ values, the canister-derived $\int[Br]dt$ values and the locally-observed O_3 mixing ratios. Error bars for the canister-derived $\int[Cl]dt$ are included on the plot and were calculated from the standard error in the slope of the linear fit (e.g., as shown in Figure 9). Similarly, error bars for the canister-derived $\int[Br]dt$ calculated from the standard error in the slope of $\ln([RH]_{obs}/[RH]_{bkg})$ against k_{Cl} and the uncertainty in $\ln([C_2H_2]_{obs}/[C_2H_2]_{bkg})$ are also shown on Figure 10. Error bars for the TOGA-derived $\int[Cl]dt$ values are not shown for clarity, but are similar in magnitude to those derived from the canisters. Slight differences existed between the $\int[Cl]dt$ values determined from the TOGA and canister data from the same time

period, primarily due to the differences in the estimated background mixing ratios for each alkane, although overall the results are very consistent between corresponding $\int[Cl]dt$ values calculated using the TOGA and canister data.

There is a clear correlation between the magnitude of the calculated $\int[Br]dt$ values and the timing of the ODEs (higher $\int[Br]dt$ during ODEs). The longest observed ODE during the study, ODE 3 between 26 and 29 March, saw a steady increase of corresponding $\int[Br]dt$ values, as well as the largest calculated $\int[Br]dt$ on 28 March at $(1.34 \pm 0.27) \times 10^{14}$ atoms cm^{-3} s (Figure S4). Interestingly, during this time period, the corresponding $\int[Cl]dt$ values were observed to peak early on 26 March and then decrease steadily throughout the duration of the ODE, demonstrating that the air mass exposures to Cl and Br are decoupled. The decrease in chlorine exposure can be understood through consideration of the Cl_2 mixing ratio results and interpretation, by *Liao et al*. [2014], who observed that ozone and light are correlated with molecular chlorine observations. During the prolonged ODE during this time period (seen most clearly in Figure 2), the air mass had been depleted of ozone for some time precluding additional formation of Cl_2 (and Cl atoms) as the air mass was transported to the site. We will discuss the evolution of Cl chemistry inside ODE 3 further in Section 3.7.

The relationship between the time-integrated halogen concentrations and local-observed ozone is shown in Figure 11, a plot of the calculated $\int[Cl]dt_{TOGA}$, $\int[Cl]dt_{can}$, and $\int[Br]dt$ against the observed O_3 mixing ratio. The relationships between the canister- and TOGA-derived $\int[Cl]dt$ and the $\int[Br]dt$ values at > 5 ppbv O_3 can be described by linear relationships

$$\int[Cl]dt_{TOGA} = [(-8.9 \pm 0.2) \times 10^7] \times [O_3] + (2.87 \pm 0.04) \times 10^9,\ r^2 = 0.474 \quad (3)$$

$$\int[Cl]dt_{can} = [(-7 \pm 1) \times 10^7] \times [O_3] + (2.4 \pm 0.2) \times 10^9,\ r^2 = 0.386 \quad (4)$$

$$\int[Br]dt_{can(O3>5\ ppbv)} = [(-3.1 \pm 0.9) \times 10^{11}] \times [O_3] + (1.0 \pm 0.2) \times 10^{13},\ r^2 = 0.312. \quad (5)$$

While the integrated Cl-atom concentrations remain relatively linear with the locally-observed ozone where ozone < 5 ppbv, there is a sharp increase in the calculated $\int[Br]dt$ with decreasing ozone. This is because at very low O_3, the dominant sinks for Br atoms are gone, so Br increases rapidly.

Figure 11 suggests that as O_3 is depleted in an air mass, the chemistry generating Cl atoms is uniform, such that the time-integrated Cl-atom exposure increases linearly, even at very low O_3, while the rapid increase of bromine atoms coinciding with the near-complete depletion of ozone is consistent with the loss of the primary Br atom sink, reaction with O_3. This is emphasized further by noting that at low O_3 mixing ratios of 5 ppbv or less, Cl-atom exposures are in the range of 2×10^9 atoms cm^{-3} s and Br-atom exposures are 10^{13} atoms cm^{-3} s or greater. Under these exposures, Br atoms destroy ozone at a rate 300 times faster than Cl atoms, clearly accounting for the majority of the O_3 destruction. At the highest calculated $\int[Br]dt$ values (~ 1×10^{14} atoms cm^{-3} s), if the duration of the bromine explosion is estimated to be one day in length, these data indicate an average Br-atom concentration of up to 1×10^9 atoms cm^{-3}. This is significantly higher than calculated in previous studies. *Jobson et al*., [1994] calculated 20 times lower Br atoms during the largest exposure of three ODEs studied, while *Ariya et al*. [1998] and *Ramacher et al*. [1999] each calculated approximately 10 times lower Br atoms during the largest exposure of the respective ODEs studied. Steady state calculations based on the data at the site [*Stephens et al*., 2012] show peak daily Br atoms ~ 1×10^9 atoms cm^{-3} during the prolonged ODE 3, consistent with our integrated Br atom exposure calculations (Figure S4).

3.5 OVOCs

3.5.1 Ketone Observations

The clean-sector acetone observations during OASIS-2009 ranged between 364 and 1531 pptv, with a mean (± standard deviation) of 800 ± 300 pptv (Table 1). There was a campaign-long increase in acetone of 17.2 ± 0.2 pptv day^{-1} (Figure 12, Table 1). A gradual increase of acetone was documented during the ALERT2000 field study [*Boudries et al.*, 2002] but an explanation was not found. The authors suggested increasing biogenic sources in the Arctic in the springtime or photochemical production from humic substances as possible, but not substantiated, explanations. We provide an interpretation of our results below.

For MEK, the clean-sector observations ranged between 59 and 296 pptv, with a mean of 190 ± 50 pptv. Over the duration of the study, there was a modest overall increase in the observed clean-sector mixing ratio of MEK of 1.30 ± 0.07 pptv day^{-1} (Figure 12, Table 1). The 2-pentanone data are the first reported measurements of this species in the Arctic. The clean-sector observations of 2-pentanone data ranged from 3 pptv to 45 pptv (Figure 12, Table 1). Unlike acetone and MEK, the observed mixing ratios of 2-pentanone experienced an overall decrease during the study, averaging -0.23 ± 0.01 pptv day^{-1}.

The observed acetone and MEK mixing ratios were moderately correlated during the study (r^2 = 0.438), as shown in Table 4 and Figure 13. It is evident from Figure 13, in which the data is colored by the date of the observations, that the relationship between acetone and MEK changed over time: during the early part of the study (warm colors), the slope ([acetone]/[MEK]) was smaller than later in the study.

The ketone results generally contrast with previous observations by *Biesenthal* [1997] and *Boudries et al*. [2002], both reporting lower mixing ratios than we report here for MEK and little correlation between the acetone and MEK with r^2 values of 0.17 and 0.13 respectively for the two studies. Both of those studies were based at Alert, however, and the proximity of Barrow to O&NG emissions may be the primary reason for the higher observed MEK values and the stronger correlation between MEK and acetone during this study.

Figure 12 reveals that acetone mixing ratios increase steadily throughout the study period from about 500 pptv to more than 1000 pptv, while MEK mixing ratios increase by only about 45 pptv over the study period. In the following sections, an explanation is explored based on the evolution of the production and loss rates of the two species during the transition from winter to spring. First we consider the production and loss of acetone.

3.6.1.1 Acetone

In this environment, acetone is formed primarily from reactions of OH and Cl with propane, isobutane and isopentane and destroyed through photolysis and reactions with OH and Cl (see Table 3 for rate coefficients). *Cavender et al*. [2008] describe the details of OH radical and halogen atom reactions of NMHC and subsequent OVOC formations and loss reactions in the Arctic. Briefly, if sufficient NO_x is available (i.e., > 50 pptv), then the acetone yield from propane (the primary source) via the 2-propyl peroxy radical is high, approximately 80% from the OH reaction and 60% from reaction with Cl [*Calvert et al*., 2011]. Under low NO_x (< 50 pptv) conditions as can be typical of the Arctic, the chemistry is more complex as the 2-propyl peroxy radical may react to a more significant extent with HO_2, typically a few pptv, to form 2-propyl hydroperoxide. This species can react further with OH and Cl, eventually forming acetone as the major product.

Early in the study, from 7 - 15 March, the approximate mixing ratios of the species of interest are: acetone (500 pptv), propane (1300 pptv), isobutane (275 pptv), and isopentane (115 pptv). Using the 24-hour average observed $J(CH_3COCH_3)$ for this time period, $\approx 3.5 \times 10^{-9}$ s^{-1}, the average of the clean-sector [OH] from this time, 3.2×10^5 molecules cm^{-3} and assuming no chlorine chemistry, the net daytime average production for acetone in early to mid-March is calculated to be approximately 1.4 pptv h^{-1} and the corresponding propane loss rate is calculated to be approximately 1.1 pptv h^{-1} (see Table 5 for a summary of these calculations). Toward the end of the study, from 1 - 14 April, the approximate mixing ratios of the species of interest are: acetone (1000 pptv), propane (500 pptv), isobutane (100 pptv), and isopentane (50 pptv). Using the average $J(CH_3COCH_3)$ from this time period, $\approx 2.2 \times 10^{-8}$ s^{-1}, and the average clean-sector observed [OH] for this time period, 4.5×10^5 molecules cm^{-3}, the average net daytime production for acetone is calculated to be 0.53 pptv h^{-1} in the absence of Cl chemistry. The corresponding propane loss rate is calculated to be 0.58 pptv h^{-1}. The propane results are in general accord with the observations that show over the course of the study an average 24 pptv day^{-1} or 1.0 pptv h^{-1} net decrease (Figure 3). For acetone, an average net increase of acetone of 17.2 pptv day^{-1} or 0.72 pptv h^{-1} (Figure 12) was observed, showing the basic trend is predicted from OH chemistry alone but at period-dependent different rates. Of course, due to the long lifetimes of propane (many weeks) and acetone (months), transport plays a large role in determining the mixing ratios that are observed at the site. Below we will explore the ramifications on these trends if chlorine atoms are present.

At the beginning of the study, even at a very modest concentration of 3.0×10^3 Cl atoms cm^{-3}, the net acetone production is calculated to more than double to 2.9 pptv h^{-1}. The corresponding calculated propane loss rate is 3.0 pptv h^{-1} or 72 pptv day^{-1}, a rate significantly higher than we observed. At the end of the study, a modest concentration of 3.0×10^3 Cl atoms cm^{-3} increases the net daytime production of acetone to 1.1 pptv h^{-1} (propane loss rate

= 1.3 pptv h^{-1}), in relatively close agreement to the overall trend rates. Differences in potential production rates due to Cl radicals between the beginning and the end of the study are chiefly due to the much higher mixing ratios of propane in the beginning (1300 pptv) compared to the end (500 pptv). Propane is responsible for more than 80% of the acetone production from alkane + Cl reactions with isobutane and isopentane responsible for the remainder of the production.

As noted earlier, measurements at the site allowed for the calculation of $[Cl]_{ss}$. The 24-hour average [Cl] calculated from the data at the site from 17 - 29 March is 3.4×10^4 atoms cm^{-3}. Using this concentration in the calculations for acetone production and propane loss, net acetone production is 18.2 pptv h^{-1} and net propane loss is 23.5 pptv h^{-1}. The data shown in Figures 3 and 12 (showing ~ 1 pptv h^{-1} production and loss for acetone and propane, respectively) do not support using the site-calculated $[Cl]_{ss}$ for the interpretation of our data and indicate that the chlorine exposures were typically less than the local [Cl] along the back trajectory of the air parcels arriving at the site. This is perhaps not surprising since a large altitude gradient is expected in the Cl-atom concentration. Longer-lived gases like propane and acetone experience less relative time exposed to chlorine atoms, which are concentrated near the surface, than shorter-lived compounds, especially those also produced at or near the snow surface. Examples are discussed below.

3.6.1.2 MEK

For MEK, the calculations are less certain because of uncertainty in the photolysis rates but in any case the production and losses are found to be in much closer balance than for acetone which experiences more production than loss throughout the study period. This helps to explain the very modest increase in [MEK] over the course of the study and hence the increase in the [acetone]/[MEK] ratio over time during the study (Figure 13). The main production pathways are via *n*-butane + OH and *n*-butane + Cl, which have yields of ≈ 0.8

and 0.6 mole mole^{-1} (248 K), respectively [*Calvert et al*., 2011; *Cavender et al*., 2008]. Similar to the propane example above, the yield of MEK from *n*-butane oxidation can be reduced under very low NO_x conditions where there is increased competition from the HO_2 radical (vs. NO) leading to hydroperoxides which can photolyze or react with OH, again eventually forming mostly MEK. MEK is lost via reactions with OH (or Cl) and by photolysis. The rate coefficients for OH with MEK and *n*-butane are not too dissimilar (Table 3), differing by only ≈ 50% and leading to similar loss rates for *n*-butane and MEK. Where Cl chemistry is active, however, because k_{Cl} for *n*-butane is about 5 times greater than for MEK, production of MEK from *n*-butane oxidation can easily outpace MEK loss.

The *n*-butane mixing ratios in the first week and last two weeks of the experiment are approximately 400 pptv and 170 pptv, respectively (Table 5). Using the average clean-sector [OH] of 3.2×10^5 molecules cm^{-3} from the beginning of the experiment and 4.5×10^5 molecules cm^{-3} at the end of the experiment, the *n*-butane lifetimes with respect to OH are 21 and 15 days, respectively. The MEK lifetime with respect to [OH] under these same scenarios is 36 and 26 days respectively. Photolysis plays a large role in the MEK lifetime, becoming more important as the study progresses. In the first week of the study the lifetime of MEK with respect to the average photolysis rate (2.4×10^{-7} s^{-1}) is ≈ 48 days, but is reduced to ≈ 12 days for the last two weeks of the study (24-hour average photolysis rate = 9.3×10^{-7} s^{-1}). Thus, the principle MEK precursor, *n*-butane, is reduced, and photolysis and hydroxyl reaction of MEK is increased as the study progresses which should lead to an overall decrease in MEK production and mixing ratios relative to the beginning of the study. Under the conditions at the beginning of the study and low [Cl], a net MEK production rate is predicted to be 0.40 pptv h^{-1}, somewhat higher than observed. Under the conditions at the end of the study and low [Cl], a net loss rate of 0.80 pptv h^{-1} is predicted whereas the observations show continued low rate production. Interestingly, near the end of the study, in the absence of

a flux from the snowpack, [Cl] > 2.0×10^4 atoms cm^{-3} is required to result in a MEK production rate greater than the loss rate. The $[Cl]_{ss}$ deduced from measurements at the site are consistent with the required amount (average $[Cl]_{ss} = 3.5 \times 10^4$ atoms cm^{-3}), but we have shown for the acetone and propane data that this amount of average sustained [Cl] is not consistent with the data. However acetone is long-lived (months) so the amount of contact during its lifetime with near-surface air where [Cl] is highest is relatively small. Conversely, the lifetime of MEK is considerably shorter and a substantial fraction of MEK is expected to be produced by Cl reactions with *n*-butane near the surface, so the relative amount of MEK exposure to Cl radicals during its lifetime should be considerably greater than that for acetone. Note also in Figure 6 that observed iC_4/C_4 ratios are enhanced during the middle and latter parts of the study compared to the earlier parts in the study indicating increased impact by Cl chemistry. The Cl_2 observations are in general accord with this assessment [*Liao et al*., 2014]. Thus, Cl radical chemistry is needed to reconcile the MEK production rates in the latter part of the study and this is qualitatively consistent with NMHC results discussed above in Section 3.5.

3.5.2 Aldehyde Observations

Acetaldehyde, propanal and butanal observed during OASIS-2009 from the clean sector varied significantly during the field campaign, ranging from below their respective detection limits to 500 pptv, 61 pptv and 54 pptv for acetaldehyde, propanal and butanal, respectively (Table 1; Figure 14). The observed aldehydes exhibited moderate correlation to each other, as listed in Table 4. For acetaldehyde and propanal, the linear least-squares fit has an r^2 value of 0.414, and the slope of an ODR fit is 4.9 ± 0.1. The ALERT2000 field study found only slight correlation between the two species ($r^2 = 0.25$, *Boudries et al*. [2002]). For butanal, abnormally high butanal mixing ratios were observed very early in the study, which could be due to instrument contamination at the site during the initial set-up, but for the

remainder of the study, the propanal and butanal were well-correlated with an overall r^2 value of 0.770.

The primary precursor for acetaldehyde in this environment is ethane, with smaller contributions from higher molecular weight hydrocarbons such as butane, pentane, and isopentane. The lifetime of acetaldehyde is quite short, especially when [Br] is large. At the beginning of the experiment and assuming OH, at an average concentration of 3.2×10^5 molecules cm^{-3}, is the primary oxidant, the lifetime is determined by reaction with OH and photolysis (average observed $J(CH_3CHO) = 1.4 \times 10^{-7}$ s^{-1}; Table 5) and is on the order of 1.5 days. At the end of the experiment, with OH as the primary oxidant ([OH] = 4.5×10^5 cm^{-3}) and the average $J(CH_3CHO) = 6.1 \times 10^{-7}$ s^{-1}, the lifetime is reduced to ~ 1 day due to increased OH reaction and photolysis. Under the early experiment scenario just described but with low [Cl] (< 10^2 atoms cm^{-3}) and [Br] (< 10^4 atoms cm^{-3}), a net chemical loss of acetaldehyde is predicted (-1.8 pptv h^{-1}). Under the late experiment scenario and the assumed low Cl and Br concentrations, a net chemical loss of acetaldehyde is also predicted (-2.1 pptv h^{-1}). Thus, if the situation were this simple, we would see essentially zero acetaldehyde coming from the clean sector.

We know, however, that large perturbations may occur in both the production of acetaldehyde from reactions of precursor NMHCs (chiefly ethane) and in the loss rates of acetaldehyde via reactions with Cl and Br atoms. This is in addition to any flux either to or from the snowpack [*Boudries et al*., 2002; *Guimbaud et al*., 2002]. As noted earlier, a wide range of halogen, radical and other measurements were made during the campaign, including chlorine molecules (Cl_2) enabling the calculation of Cl atom concentrations at the site [*Liao et al*., 2014, *Stephens et al*., 2012]. At noon, $[Cl]_{ss} = 2 \times 10^5$ atoms cm^{-3} was predicted, which is a surprisingly high number. Average daytime molecular chlorine levels were correlated with ozone concentrations, suggesting that sunlight and ozone are required for molecular

chlorine formation in the ambient atmosphere. This has strong implications for the chemistry occurring at the site. Because Cl reacts efficiently with ethane which is always present in the Arctic atmosphere at high levels (~ 2 ppbv; Figure 3), the clean-sector aldehyde mixing ratios might be expected to follow the O_3 mixing ratios and this is what is generally observed (Figure 14). It should be noted that testing of the TOGA instrument showed little indications of artifacts from ozone interferences (Text S1) and thus measurement issues and instrument artifacts can be ruled out as a major contributing cause of any observed correlation between aldehydes and ozone shown in Figure 14. At noontime with [Cl] = 2×10^5 atoms cm^{-3}, at 1.5 m above snow surface (the height of the halogen measurements) the net production of acetaldehyde from ethane minus the loss of acetaldehyde via reaction with Cl is predicted to be 73 pptv h^{-1}, a very large chemical flux (6.1×10^5 molecules cm^{-3} s^{-1}). Using the average calculated Cl (over the period of 17 March – 1 April) the net acetaldehyde production at the site at 1.5 m is predicted to be 11 pptv h^{-1}.

It is known from the literature that Br atoms are largely responsible for ODEs widely observed in the Arctic including this experiment [*Thompson et al*., 2015]. It is also known from laboratory kinetics studies that the aldehydes react more quickly with Br atoms than does ozone (Table 3). It is possible to calculate the net acetaldehyde chemical production or destruction at the site considering all three oxidants simultaneously: measured [OH] and calculated $[Br]_{ss}$ and $[Cl]_{ss}$. During the extended ODE 3, the midday $[Br]_{ss}$ levels are near 1.0×10^9 cm^{-3}. The aldehydes have little chance to survive under these conditions as destruction rates are very large (> 100 pptv h^{-1} or 8.84×10^5 molecules cm^{-3} s^{-1} for CH_3CHO; assuming [CH_3CHO] = 10 pptv; and even higher destruction rates for propanal and butanal). The lifetime of acetaldehyde under these conditions is only 340 seconds. In the relatively stable atmosphere at Barrow, an effective mixing height Z* may be defined [*Guimbaud et al*., 2002; *Lenschow*, 1995] as the vertical distance traveled during one lifetime, τ:

$$Z^* = (K_c \tau)^{1/2} \quad (6)$$

where K_c is the regular, average eddy diffusivity. For this time period, 26 – 29 March, K(1.8 m) ≈ 1000 $cm^2 s^{-1}$, thus, for acetaldehyde, Eq. (6) yields Z* ~ 6 m. Extremely rapid chemistry is occurring within this mixing height when halogen atoms are present. Ethane is rapidly forming acetaldehyde from reaction with Cl and acetaldehyde is even more rapidly destroyed by Br atoms. Similarly, under these conditions, propanal and butanal are rapidly formed from reactions of propane and butane with Cl atoms, while being more rapidly destroyed via reactions with Cl and Br atoms.

The data in Figure 14 show that indeed during the ODEs, acetaldehyde and the other aldehyde mixing ratios approach or are equal to zero, such that all three aldehydes show significant correlations with O_3 during the study (r^2 values = 0.542, 0.563 and 0.533 for acetaldehyde, propanal and butanal, respectively; Figure S5). Although this complete or near-complete depletion of aldehydes has never been previously observed, this is what we expect based on the kinetic considerations above. Some effect of Br atom chemistry on aldehydes has been previously reported. During the ALERT2000 field campaign, acetaldehyde was measured within the snowpack interstitial air and in the boundary layer [*Boudries et al*., 2002; *Guimbaud et al*., 2002]. A correlation with ozone was observed and attributed to Br atom processing but the high loss rates that were calculated with the mixing ratios they observed were never reconciled despite their observation of a significant flux of acetaldehyde from the snowpack. In their study, three ODEs were observed during the light period and acetaldehyde reached only a minimum value of 26 pptv (well above the 8 pptv detection limit). Similarly, from a previous Alert campaign, *Sumner and Shepson* [1999] reported HCHO minimizing when O_3 was near zero. The data we present are the first that definitively show aldehyde depletion coinciding with ODEs.

The snowpack has been shown to be an additional source of aldehydes in the Arctic [*Boudries et al*., 2002; *Grannas et al*., 2002; *Guimbaud et al*., 2002]. As well, fluxes from the snow have been inferred from diel profiles of OVOC mixing ratios and the impact of snowpack source [*Grannas et al*., 2002]. In our data we see very slight diel variations for the aldehydes, with maximum mixing ratios during the 12:00 – 15:00 AKST time period (Figure S6). Nevertheless, considering only the gas-phase chemistry, the chemical fluxes for aldehydes in the Arctic boundary layer are significant given the high Cl-atom concentrations (as calculated by *Liao et al*. [2014]). Distributing the acetaldehyde chemical flux determined above, 6.1×10^5 molecules cm^{-3} s^{-1}, into a layer with effective mixing height 6 m for the purpose of comparing with reported surface fluxes gives a value of 3.6×10^8 molecules cm^{-2} s^{-1}, comparable in magnitude to the non-ODE acetaldehyde snow-air fluxes reported by *Guimbaud et al*. [2002] (4.2×10^8 molecules cm^{-2} s^{-1}) and *Boudries et al*. [2002] (2.6×10^9 molecules cm^{-2} s^{-1}).

4. Conclusions

The VOC observations made using the TOGA at Barrow, Alaska during the OASIS-2009 field campaign contributed an extensive and unprecedented data set of both NMHC and OVOCs in the high Arctic, complemented by the inclusion of whole air canister measurements. Strong correlations exist between the NMHC observed at the site, which are influenced to varying degrees by regional O&NG extraction operations, in particular the large Prudhoe Bay oil field, approximately 300 km ESE of the field site. During the study, observed clean-sector NMHCs and aldehydes demonstrated an overall decrease in mixing ratios with time whereas acetone and MEK showed increases. The decrease in NMHCs is consistent with the Arctic seasonality and is primarily due to the increase in OH reactions during the study but with clear influences from halogen radical chemistry. The ratios of

isobutane/*n*-butane demonstrated that Cl chemistry played a significant role in processing the VOCs, including the NMHCs, and that the influence from Cl increased during the study. The increases and trends in acetone and MEK can be explained primarily from OH chemistry acting on precursors but with a contribution from Cl chemistry, particularly later in the study, which maintains the formation rate of the ketones despite the lower concentration of precursors.

Several ODEs were observed during the study, providing an opportunity to investigate the impact of halogen chemistry on NMHC ratios, and likewise, to use NMHC to investigate the integrated history of halogen chemistry of the air masses observed. From the longest-observed ODE of the campaign, the calculations of time-integrated concentrations of Br atoms, $\int[Br]dt$, yielded values greater than 10^{14} cm^{-3} s, a higher value than ever previously observed. Extensive chemical and radical measurements at the site allowed for the calculation of steady-state concentrations of Br and Cl radicals. The $[Br]_{ss}$ calculated at the site correlated well with $\int[Br]dt$ during the longest extended ODE with $\int[Br]dt$ levels virtually equivalent with $[Br]_{ss}$ if a one-day exposure is assumed.

The chemistry of the C_2-C_4 aldehydes (i.e., acetaldehyde, propanal and butanal) was explored. These very reactive, short-lived species have been the subject of a number of studies but none with the benefit of the wide array of measurements that were available for OASIS-2009. A kinetic analysis showed that the high radical concentrations ($[Br]_{ss}$ and $[Cl]_{ss}$) calculated from measurements at the site provide for extremely vigorous chemistry. High concentrations of calculated chlorine radicals (2×10^5 atoms cm^{-3} at midday) are responsible for a large chemical flux of C_2-C_4 aldehydes near the snow surface from reactions of NMHC precursors (primarily ethane, propane and *n*-butane), which could make it difficult to distinguish chemical fluxes from snow-air fluxes. However, during ODEs when Br atoms

reach ≈ 2×10^5 atoms cm^{-3}, the aldehydes, being more reactive with Br than ozone, are quickly destroyed, resulting in aldehyde depletion events coinciding with ODEs.

5. Acknowledgements

Additional support to NCAR under NSF grant 0806437 is gratefully acknowledged. The authors wish to thank the organizers of the OASIS-2009 field campaign, the Barrow Arctic Science Consortium for logistics support, and all of the researchers who contributed to the campaign. Thanks are also expressed to Audra McClure-Begley and Irina Petropavlovskikh for the provision of NOAA Barrow Observatory data. The authors also thank Mary Barth, Geoff Tyndall and six anonymous reviewers for their insightful comments and suggestions. The National Center for Atmospheric Research is sponsored by the National Science Foundation. Any opinions, findings and conclusions or recommendations expressed in the publication are those of the authors and do not necessarily reflect the views of the National Science Foundation. All data from the OASIS Barrow 2009 field campaign are publicly available at http://dx.doi.org/10.5065/D6CJ8BM3.

6. References

Anastasio, C., and T. Robles (2007), Light absorption by soluble chemical species in Arctic and Antarctic snow, J. Geophys. Res., 112, D24304, doi: 10.1029/2007JD008695.

Apel, E. C., J. G. Calvert, and F. C. Fehsenfeld (1994), The Nonmethane Hydrocarbon Intercomparison Experiment (NOMHICE): Tasks 1 and 2, J. Geophys. Res., 99(D8), 16651–16664, doi: 10.1029/94JD00086.

Apel, E. C., J. G. Calvert, R. Zika, M. O. Rodgers, V. P. Aneja, J. F. Meagher, and W. A. Lonneman (1995), Hydrocarbon measurements during the 1992 Southern Oxidants Study Atlanta intensive: protocol and quality assurance, J. Air Waste Manag. Assoc., 45(7), 521-528, doi: 10.1080/10473289.1995.10467383.

Apel, E. C., J. G. Calvert, J. P. Greenberg, D. Riemer, R. Zika, T. E. Kleindienst, W. A. Lonneman, K. Fung, and E. Fujita (1998a), Generation and validation of oxygenated volatile organic carbon standards for the 1995 Southern Oxidants Study Nashville Intensive, J. Geophys. Res., 103(D17), 22281–22294, doi: 10.1029/98JD01383.

Apel, E. C., J. G. Calvert, D. Riemer, W. Pos, R. Zika, T. E. Kleindienst, W. A. Lonneman, K. Fung, E. Fujita, P. B. Shepson, T. K. Starn, and P. T. Roberts (1998b), Measurements comparison of oxygenated volatile organic compounds at a rural site during the 1995 SOS Nashville Intensive, J. Geophys. Res., 103, 22,295 – 22,316, doi: 10.1029/98JD01753.

Apel, E. C., J. G. Calvert, T. M. Gilpin, F. C. Fehsenfeld, D. D. Parrish, and W. A. Lonneman (1999), The Nonmethane Hydrocarbon Intercomparison Experiment (NOMHICE): Task 3, J. Geophys. Res., 104(D21), 26069–26086, doi: 10.1029/1999JD900793.

Apel, E. C., A. J. Hills, R. Lueb, S. Zindel, S. Eisele, and D. D. Riemer (2003), A fast-GC/MS system to measure C_2 to C_4 carbonyls and methanol aboard aircraft, J. Geophys. Res., 108(D20), 8794, doi: 10.1029/2002JD003199.

Apel, E. C., T. Brauers, R. Koppmann, B. Bandowe, J. Boßmeyer, C. Holzke, R. Tillmann, A. Wahner, R. Wegener, A. Brunner, M. Jocher, T. Ruuskanen, C. Spirig, D. Steigner, R. Steinbrecher, E. Gomez Alvarez, K. Müller, J. P. Burrows, G. Schade, S. J. Solomon, A. Ladstätter-Weißenmayer, P. Simmonds, D. Young, J. R. Hopkins, A. C. Lewis, G. Legreid, S. Reimann, A. Hansel, A. Wisthaler, R. S. Blake, A. M. Ellis, P. S. Monks, K. P. Wyche. (2008), Intercomparison of oxygenated volatile organic compound measurements at the SAPHIR atmosphere simulation chamber, J. Geophys. Res., 113, D20307, doi: 10.1029/2008JD009865.

Apel, E. C., L. K. Emmons, T. Karl, F. Flocke, A. J. Hills, S. Madronich, J. Lee-Taylor, A. Fried, P. Weibring, J. Walega, D. Richter, X. Tie, L. Mauldin, T. Campos, A. Weinheimer, D. Knapp, B. Sive, L. Kleinman, S. Springston, R. Zaveri, J. Ortega, P. Voss, D. Blake, A. Baker, C. Warneke, D. Welsh-Bon, J. de Gouw, J. Zheng, R. Zhang, J. Rudolph, W. Junkermann, and D. D. Riemer (2010), Chemical evolution of volatile organic compounds in the outflow of the Mexico City Metropolitan area, Atmos. Chem. Phys., 10, 2353-2376, doi: 10.5194/acp-10-2353-2010.

Apel, E. C., R. S. Hornbrook, A. J. Hills, N. J. Blake, M. C. Barth, A. Weinheimer, C. Cantrell, S. A. Rutledge, B. Basarab, J. Crawford, G. Diskin, C. R. Homeyer, T. Campos, F. Flocke, A. Fried, D. R. Blake, W. Brune, I. Pollack, J. Peischl, T. Ryerson, P. O. Wennberg, J. D. Crounse, A. Wisthaler, T. Mikoviny, G. Huey, B. Heikes, D. O'Sullivan, and D. D. Riemer (2015), Upper tropospheric ozone production from lightning NO_x-impacted convection: Smoke ingestion case study from the DC3 campaign. J. Geophys. Res. Atmos., 120, 2505–2523. doi: 10.1002/2014JD022121.

Ariya, P. A., B. T. Jobson, R. Sander, H. Niki, G. W. Harris, J. F. Hopper, and K. G. Anlauf (1998), Measurements of C_2-C_7 hydrocarbons during the Polar Sunrise Experiment 1994: Further evidence for halogen chemistry in the troposphere, J. Geophys. Res., 103(D11), 13169-13180, doi: 10.1029/98JD00284.

Atkinson, R., D. L. Baulch, R. A. Cox, J. N. Crowley, R. F. Hampson, R. G. Hynes, M. E. Jenkin, M. J. Rossi, and J. Troe (2006), Evaluated kinetic and photochemical data for atmospheric chemistry: Volume II – gas reactions of organic species, Atmos. Chem. Phys., 6, 3625-4055, doi: 10.5194/acp-6-3625-2006.

Atkinson, R., D. L Baulch, R. A. Cox, J. N. Crowley, R. F. Hampson, R. G. Hynes, M. E. Jenkin, M. J. Rossi, and J. Troe (2007), Evaluated kinetic and photochemical data for atmospheric chemistry: Volume III – gas reactions of inorganic halogens, Atmos. Chem. Phys., 7, 981-1191, doi: 10.5194/acp-7-981-2007.

Barret, M., F. Dominé, S. Houdier, J.-C. Gallet, P. Weibring, J. Walega, A. Fried, and D. Richter (2011), Formaldehyde in the Alaskan Arctic snowpack: Partitioning and physical processes involved in air-snow exchanges, J. Geophys. Res., 116(D00R03), 116, D00R03, doi: 10.1029/2011JD016038.

Barrie, L. A., J. W. Bottenheim, R. C. Schnell, P. J. Crutzen, and R. A. Rasmussen (1988), Ozone destruction and photochemical reactions at polar sunrise in the lower Arctic atmosphere, Nature, 334, 138-141, doi: 10.1038/334138a0.

Beine, H. J., R. E. Honrath, F. Dominé, W. R. Simpson, and J. D. Fuentes (2002), NO_x during background and ozone depletion events at Alert: Fluxes above the snow surface, J. Geophys. Res., 107(D21), doi: 10.1029/2002JD002082.

Beine, H., A. J. Colussi, A. Amoroso, G. Esposito, M. Montagnoli, and M. R. Hoffmann (2008), HONO emissions from snow surfaces, Environ. Res. Lett. 3, 045005, doi: 10.1088/1748-9326/3/4/045005.

Biesenthal, T. A. (1997), The role of carbonyl compounds in tropospheric ozone chemistry, Ph.D. Thesis, Department of Chemistry, York University, Toronto, Canada.

Bottenheim, J. W., A. G. Gallant, and K. A. Brice (1986), Measurements of NO_y species and O_3 at 82° latitude, Geophys. Res. Lett., 13(2), doi: 10.1029/GL013i002p00113.

Boudries, H., and J. W. Bottenheim (2000), Cl and Br atom concentrations during a surface boundary layer ozone depletion event in the Canadian high Arctic, Geophys. Res. Lett., 27(4), 517-510, doi: 10.1029/1999GL011025.

Boudries, H., J. W. Bottenheim, C. Guimbaud, A. M. Grannas, P. B. Shepson, S. Houdier, S. Perrier, and F. Dominé (2002), Distribution and trends of oxygenated hydrocarbons in the high Arctic derived from measurements in the Atmospheric boundary layer and interstitial snow air during the ALERT2000 field campaign, Atmos. Environ., 36, doi: 10.1016/S1352-2310(02)00122-X.

Boylan, P., D. Helmig, R. Staebler, A. Turnipseed, C. Fairall, and W. Neff (2013), Boundary layer dynamics during the Ocean-Atmosphere-Sea-Ice-Snow (OASIS) 2009 Experiment at Barrow, AK, J. Geophys. Res., 119(5), 2261-2278, doi: 10.1002/2013JD020299.

Calvert, J. G., A. Mellouki, J. J. Orlando, M. J. Pilling, and T. J. Wallington (2011), Mechanisms or Atmospheric Oxidation of the Oxygenates, New York: Oxford University Press.

Calvert, J. G., J. J. Orlando, W. R. Stockwell, and T. J. Wallington (2015), The Mechanisms of Reactions Influencing Atmospheric Ozone, New York: Oxford University Press.

Cavender, A. E., T. A. Biesenthal, J. W. Bottenheim, and P. B. Shepson (2008), Volatile organic compound ratios as probes of halogen atom chemistry in the Arctic, Atmos. Chem. Phys., 8, 1737-1750, doi: 10.5194/acp-8-1737-2008.

Dibb, J. E., and M. Arsenault (2002), Shouldn't snowpacks be sources of monocarboxylic acids? Atmos. Environ., 36, 2513-2522, doi: 10.1016/S1352-2310(02)00131-0.

Dibb J. E., L. G. Huey, D. L. Slusher, and D. J. Tanner (2004), Soluble reactive nitrogen oxides at South Pole during ISCAT 2000, Atmos. Environ., 38(32), 5399-5409, doi: 10.1016/j.atmosenv.2003.01.001.

Dominé, F. and P. B. Shepson (2002), Air-snow interactions and atmospheric chemistry, Science, 297(5586), 1506-510, doi: 10.1126/science.1074610.

Doskey, P. V. and J. S. Gaffney (1992), Non-methane hydrocarbons in the Arctic atmosphere at Barrow, Alaska, J. Geophys. Res., 19(4), 381-384, doi: 10.1029/91GL03136.

Draxler, R. R., and G. D. Rolph (2015), HYSPLIT (HYbrid Single-Particle Lagrangian Integrated Trajectory) Model access via NOAA ARL READY Website (http://ready.arl.noaa.gov/HYSPLIT.php). NOAA Air Resources Laboratory, Silver Spring, MD.

Fan, S-M., and D. J. Jacob (1992), Surface ozone depletion in Arctic spring sustained by bromine reactions on aerosols, Nature, 359, 522–524, doi: 10.1038/359522a0.

Finlayson-Pitts, B. J., F. E. Livingston, and H. N. Berko (1990), Ozone destruction and bromine photochemistry at ground level in the Arctic spring, Nature, 343, 622-625, doi: 10.1038/343622a0.

Foster, K. L., R. A. Plastridge, J. W. Bottenheim, P. B. Shepson, B. J. Finlayson-Pitts and C. W. Spicer (2001), First tropospheric measurements of Br_2 and BrCl and their role in surface ozone destruction at polar sunrise, Science, *291*, 471-474 doi: 10.1126/science.291.5503.471.

Galbavy, E. S., C. Anastasio, B. Lefer, and S. Hall (2007), Light Penetration in the Snowpack at Summit, Greenland: Part 1. Nitrite and Hydrogen Peroxide Photolysis, Atmospheric Environment, 41(24), 5077-5090, doi: 10.1016/j.atmosenv.2006.04.072

Gautrois, M., T. Brauers, R. Koppmann, F. Rohrer, O. Stein, and J. Rudolph (2003), Seasonal variability and trends of volatile organic compounds in the lower polar troposphere, J. Geophys. Res., 108(D13), 4393, doi: 10.1029/2002JD002765.

Gilman, J. B., J. F. Burkhart, B. M. Lerner, E. J. Williams, W. C. Kuster, P. D. Goldan, P. C. Murphy, C. Warneke, C. Fowler, S. A. Montzka, B. R. Miller, L. Miller, S. J. Oltmans, T. B. Ryerson, O. R. Cooper, A. Stohl., and J. A. de Gouw (2010), Ozone variability and halogen oxidation within the Arctic and sub-Arctic springtime boundary layer, Atmos. Chem. Phys., 10, 10223-10236, doi: 10.5194/acp-10-10223-2010.

Gilman, J. B., Lerner, B. M., Kuster, W. C., and de Gouw, J. A., Source signature of volatile organic compounds from oil and natural gas operations in Northeastern Colorado (2013), Environ. Sci. Technol., 47(3), 1297-1305, doi: 10.1021/es304119a.

Grannas, A. M., P. B. Shepson, C. Guimbaud, A. L. Sumner, M. Albert, W. Simpson, F. Dominé, H. Boudries, J. Bottenheim, H. J. Beine, R. Honrath, and X. Zhou (2002), A study of photochemical and physical processes affecting carbonyl compounds in the Arctic atmospheric boundary layer, Atmos. Environ., 36, 2733-2742, doi: 10.1016/S1352-2310(02)00122-X.

Grannas, A. M., A. E. Jones, J. Dibb, M. Ammann, C. Anastasio, H. J. Beine, M. Bergin, J. Bottenheim, C. S. Boxe, G. Chen, J. H. Crawford, F. Dominé, M. M. Frey, M. I. Guzmán,

D. E. Heard, D. Helmig, M. R. Hoffmann, R. E. Honrath, L. G. Huey, M. Hutterli, H. W. Jacobi, P. Klán, B. Lefer, J. McConnell, J. Plane, R. Sander, J. Savarino, P. B. Shepson, W. R. Simpson, J. R. Sodeau, R. von Glasow, R. Weller, E. W. Wolff, and T. Zhu (2007), An overview of snow photochemistry: evidence, mechanisms and impacts, Atmos. Chem. Phys., 7, 4329-4373, doi: 10.5194/acp-7-4329-2007.

Guenther, A. B., and A. J. Hills (1998), Eddy covariance measurement of isoprene fluxes, J. Geophys. Res.,103, 13,145–13,152, doi: 10.1029/97JD03283.

Guimbaud, C., A. M. Grannas, P. B. Shepson, J. D. Fuentes, H. Boudries, J. W. Bottenheim, F. Dominé, S. Houdier, S. Perrier, T. B. Biesenthal, and B. G. Splawn (2002), Snowpack processing of acetaldehyde and acetone in the Arctic atmospheric boundary layer, Atmos. Environ., 36, 2743-2752, doi: 10.1016/S1352-2310(02)00107-3.

Helmig, D., P. Boylan, P., B. Johnson, S. Oltman, C. Fairall, R. Staebler, A. Weinheimer, J. Orlando, D. J. Knapp, D. D. Montzka, F. Flocke, U. Frieß, H. Sihler, and P. B. Shepson (2012), Ozone dynamics and snow-atmosphere exchanges during ozone depletion events at Barrow, Alaska, J. Geophys. Res., 117(D20303), doi: 10.1029/2012JD017531.

Helmig, D., C. R. Stephens, J. Caramore, and J. Hueber (2014), Seasonal behavior of non-methane hydrocarbons in the firn air at Summit, Greenland, Atmos. Environ., 85, 234-246, doi: 10.1016/j.atmosenv.2013.11.021.

Honrath, R. E., M. C. Peterson, S. Guo, J. E. Dibb, P. B. Shepson, and B. Campbell (1999), Evidence of NO_x production within or upon ice particles in the Greenland snowpack, Geophys. Res. Lett., 26(6), 695-698, doi: 10.1029/1999FL900077.

Honrath, R. E., Y. Lu, M. C. Peterson, J. E. Dibb, M. A. Arsenault, N. J. Cullen, and K. Steffen (2002), Vertical fluxes of NO_x, HONO, and HNO_3 above the snowpack at Summit, Greenland, Atmos. Environ., 36, 2629-2640, doi: 10.1016/S1352-2310(02)00132-2.

Hornbrook, R. S., D. R. Blake, G. S. Diskin, A. Fried, H. E. Fuelberg, S. Meinardi, T. Mikoviny, D. Richter, G. W. Sachse, S. A. Vay, J. Walega, P. Weibring, A. J. Weinheimer, C. Wiedinmyer, A. Wisthaler, A. Hills, D. D. Riemer, and E. C. Apel (2011), Observations of nonmethane organic compounds during ARCTAS − Part 1: Biomass burning emissions and plume enhancements, Atmos. Chem. Phys., 11, 11103-11130, doi: 10.5194/acp-11-11103-2011.

Houdier, S., S. Perrier, F. Dominé, A. Cabanes, L. Legagneux, A. M. Grannas, C. Guimbaud, P. B. Shepson, H. Boudries, and J. W. Bottenheim (2002), Acetaldehyde and acetone in the Arctic snowpack during the ALERT2000 campaign. Snowpack composition, incorporation processes and atmospheric impact, Atmos. Environ., 36, 2609-2618, doi: 10.1016/S1352-2310(02)00107-3.

Hutterli, M. A., R. Röthlisberger, and R. C. Bales (1999), Atmosphere-to-snow-to-firn transfer studies of HCHO at Summit, Greenland, Geophys. Res. Lett., 26(12), 1691–1694, doi: 10.1029/1999GL900327.

Hutterli, M. A., R. C. Bales, J. R. McConnell, and R. W. Stewart (2002), HCHO in Antarctic snow: Preservation in ice cores and air-snow exchange, Geophys. Res. Lett., 29(8), 1235, doi: 10.1029/2001GL014256.

Impey, G. A., P. B. Shepson, D. R. Hastie, L. A. Barrie, and K. G. Anlauf (1997), Measurements of photolyzable chlorine and bromine during the Polar Sunrise Experiment 1995, J. Geophys. Res., 102(D13), 16,005-16,010, doi: 10.1029/97JD00851.

Jacobi, H.-W., M. M. Frey, M. A. Hutterli, R. C. Bales, O. Schrems, N. J. Cullen, K. Steffen, and C. Koehler (2002), Measurements of hydrogen peroxide and formaldehyde exchange between the atmosphere and surface snow at Summit, Greenland, Atmos. Environ., 36(15-16), 2619-2628, doi: 10.1016/S1352-2310(02)00106-1.

Jaffe, D. A., R. E. Honrath, J. A. Herring, S.-M. Li, and J. D. Kahl (1991), Measurements of nitrogen oxides at Barrow, Alaska during spring: Evidence for regional and northern hemispheric sources of pollution, J. Geophys. Res., 96(D4), 7395–7405, doi: 10.1029/91JD00065.

Jobson, B. T., H. Niki, Y. Yokouchi, J. Bottenheim, F. Hopper, F., and R. Leaitch (1994), Measurements of C_2-C_6 hydrocarbons during the Polar Sunrise 1992 Experiment: Evidence for Cl and Br atom chemistry, J. Geophys. Res., 99(D12), 25,355-25,368, doi: 10.1029/94JD01243.

Kramer, L. J., D. Helmig, J. F. Burkhart, A. Stohl, S. Oltmans, and R. E. Honrath (2015), Seasonal variability of atmospheric nitrogen oxides and non-methane hydrocarbons at the GEOSummit station, Greenland, Atmos. Chem. Phys., 15, 6827-6849, doi: 10.5194/acp-15-6827-2015.

Lee-Taylor, J., and S. Madronich (2002), Calculation of actinic fluxes with a coupled atmosphere-snow radiative transfer model, J. Geosphy. Res. 107(D24), 4796, doi: 10.1029/2002JD002084.

Lenschow, D.H. (1995) Micrometeorological techniques for measuring biosphere–atmosphere trace gas exchange, in Biogenic Trace Gases: Measuring Emissions from Soil and Water, pp. 126-163, Blackwell Science, Oxford, England.

Liao, J., H. Sihler, L. G. Huey, J. A. Neuman, D. J. Tanner, U. Friess, U. Platt, F. M. Flocke, J. J. Orlando, P. B. Shepson, H. J. Beine, A. J. Weinheimer, S. J. Sjostedt, J. B. Nowak, D. J. Knapp, R. M. Staebler, W. Zheng, R. Sander, S. R. Hall, and K. Ullmann (2011), A comparison of Arctic BrO measurements by chemical ionization mass spectrometry and lon path-differential optical absorption spectroscopy, J. Geophys. Res., 116(D00R02), doi: 10.1029/2010JD014788.

Liao, J., L. G. Huey, Z. Liu, Z., D. J. Tanner, C. A. Cantrell, J. J. Orlando, F. M. Flocke, P. B. Shepson, A. J. Weinheimer, S. R. Hall, K. Ullmann, H. J. Beine, Y. Wang, E. D. Ingall, C. R. Stephens, R. S. Hornbrook, E. C. Apel, D. Riemer, A. Fried, R. L. Mauldin III, J. N. Smith, R. M. Staebler, J. A. Neuman, and J. B. Nowak (2014), High levels of molecular chlorine in the Arctic atmosphere, Nat. Geosci., 7, 91-94, doi: 10.1038/ngeo2046.

Mauldin III, R. L., D. J. Tanner, and F. L. Eisele (1999), Measurements of OH during PEM-Tropics A, J. Geophys. Res., 104(D5), 5817-5827, doi: 10.1029/98JD02305.

McClure-Begley, A., I. Petropavlovskikh, and S. Oltmans (2014), NOAA Global Monitoring Surface Ozone Network. 1973-2014. National Oceanic and Atmospheric Administration, Earth Systems Research Laboratory Global Monitoring Division, Boulder, CO, (02/15/2011), doi: 10.7289/V57P8WBF.

McConnell, J. C., G. S. Henderson, L. Barrie, J. Bottenheim, H. Niki, C. H. Langford, and E. M. J. Templeton (1992), Photochemical bromine production implicated in Arctic boundary-layer ozone depletion, Nature, 355, 150-152, doi: 10.1038/355150a0.

Oltmans, S. J., and W. D. Komhyr (1986), Surface ozone distributions and variations from 1973-1984 measurements at the NOAA Geophysical Monitoring for Climatic Change Baseline Observatories, J. Geophys. Res., 91(D4), 5229-5236, doi: 10.1029/JD091iD04p05229.

Oltmans, S. J., B. J. Johnson, and J. M. Harris (2012), Springtime boundary layer ozone depletion at Barrow, Alaska: Meteorological influence, year-to-year variation, and long-term change, J. Geophys. Res., 117, D00R18, doi: 10.1029/2011JD016889.

Pratt, K. A., K. D. Custard, P. B. Shepson, T. A. Douglas, D. Pöhler, S. General, J. Zielcke, W. R. Simpson, U. Platt, D. J. Tanner, L. G. Huey, M. Carlson, and B. H. Stirm (2013), Photochemical production of molecular bromine in Arctic surface snowpacks, Nat. Geosci., 6, 351-356, doi: 10.1038/ngeo1779.

Ramacher, B., J. Rudolph, and R. Koppmann (1999), Hydrocarbon measurements during tropospheric ozone depletion events: Evidence for halogen atom chemistry, J. Geophys. Res., 104(D3), 3633–3653, doi:10.1029/1998JD100061.Ramacher, B., J. J. Orlando, and G. S. Tyndall (2000), Temperature-dependent rate coefficient measurements for the reaction of bromine atoms with a series of aldehydes, Int. J. Chem. Kinet., 32(8), 460-465, doi: 10.1002/1097-4601(2000)32:8<460::AID-KIN2>3.0.CO;2-P.

Reinmann, S., R. Kallenborn, and N. Schmidbauer (2009), Severe aromatic hydrocarbon pollution of Arctic town of Longyearbyen (Svalbard) caused by snowmobile emissions, Environ. Sci. Technol., 43, 4791-4795, doi: 10.1021/es900449x.

Ridley, B. A., and F. E. Grahek (1990), A small, low flow, high sensitivity reaction vessel for NO chemiluminescence detectors, J. Atmos. Oceanic Technol., 7, 307–311, doi: 10.1175/1520-0426(1990)007<0307:ASLFHS>2.0.CO;2.

Ridley, B. A., F. E. Grahek, and J. G. Walega (1992), A small, high-sensitivity, medium-response ozone detector suitable for measurements from light aircraft, J. Atmos. Oceanic Technol., 9(2), 142–148, doi: 10.1175/1520-0426(1992)009<0142:ashsmr>2.0.co;2.

Rolph, G.D., (2015) Real-time Environmental Applications and Display sYstem (READY) Website (http://ready.arl.noaa.gov). NOAA Air Resources Laboratory, Silver Spring, MD.

Rudolph, J., B. R. Fu, A. Thompson, K. Anlauf, and J. Bottenheim (1999), Halogen atom concentration in the Arctic troposphere derived from hydrocarbon measurements: impact on the budget of formaldehyde, Geophys. Res. Lett., 26(19), 2941-2944, doi: 10.1029/1999GL010869.

Russo, R. S., Y. Zhou, K. B. Haase, O. W. Wingenter, E. K. Frinak, H. Mao, R. W. Talbot, and B. C. Sive (2010a), Temporal variability, sources, and sinks of C_1-C_5 alkyl nitrates in coastal New England, Atmos. Chem. Phys., 10, 1865–1883, doi: 10.5194/acp-10-1865-2010.

Russo, R. S., Y. Zhou, M. L. White, H. Mao, R. Talbot, and B. C. Sive (2010b), Multi-year (2004–2008) record of nonmethane hydrocarbons and halocarbons in New England:

Seasonal variations and regional sources, Atmos. Chem. Phys., 10, 4909–4929, doi: 10.5194/acp-10-4909-2010.

Salmon, R. A., S. J.-B. Bauguitte, W. Bloss, M. A. Hutterli, A. E. Jones, K. Read, and E. W. Wolff (2008), Measurement and interpretation of gas phase formaldehyde concentrations obtained during the CHABLIS campaign in coastal Antarctica, Atmos. Chem. Phys., 8, 4085-4093, doi: 10.5194/acp-8-4085-2008.

Shetter, R. E., and M. Muller (1999), Photolysis frequency measurements using actinic flux spectroradiometry during the PEM-Tropics mission: Instrumentation description and some results, J. Geophys. Res., 104(D5), 5647-5661, doi: 10.1029/98JD01381.

Simpson, I. J., N. J. Blake, B. Barletta, G. S. Diskin, H. E. Fuelberg, K. Gorham, L. G. Huey, S. Meinardi, F. S. Rowland, S. A. Vay, A. J. Weinheimer, M. Yang, and D. R. Blake (2010), Characterization of trace gases measured over Alberta oil sands mining operations: 76 speciated C_2-C_{10} volatile organic compounds (VOCs), CO_2, CH_4, CO, NO, NO_2, NO_y, O_3 and SO_2, Atmos. Chem. Phys., 10, 11931-11954, doi: 10.5194/acp-10-11931-2010.

Simpson, W. R., R. von Glasow, K. Riedel, P. Anderson, P. Ariya, J. Bottenheim, J. Burrows, L. J. Carpenter, U. Frieß, M. E. Goodsite, D. Heard, M. Hutterli, H.-W. Jacobi, L. Kaleschke, B. Neff, J. Plane, U. Platt, A. Richter, H. Roscoe, R. Sander, P. Shepson, J. Sodeau, A. Steffen, T. Wagner, and E. Wolff (2007), Halogens and their role in polar boundary-layer ozone depletion, Atmos. Chem. Phys., 7, 4375-4413, doi: 10.5194/acp-7-4375-2007.

Sive, B. C., Y. Zhou, D. Troop, Y. Wang, W. C. Little, O. W. Wingenter, R. S. Russo, R. K. Varner, and R. Talbot (2005), Development of a cryogen-free concentration system for measurements of volatile organic compounds, Anal. Chem., 77, 6989-6998, doi: 10.1021/ac0506231.

Stephens, C. R., P. B. Shepson, A. Steffen, J. W. Bottenheim, J. Liao, L. G. Huey, E. Apel, A. Weinheimer, S. R. Hall, C. Cantrell, B. C. Sive, D. J. Knapp, D. D. Montzka, and R. S. Hornbrook (2012), The relative importance of chlorine and bromine radicals in the oxidation of atmospheric mercury at Barrow, Alaska, J. Geophys. Res., 117, D00R11, doi: 10.1029/2011JD016649.

Sumner, A. L., and P. B. Shepson (1999), Snowpack production of formaldehyde and its effect on the Arctic troposphere, Nature, 398, 230-233, doi: 10.1038/18423.

Swanson, A. L., N. J. Blake, E. Atlas, F. Flocke, D. R. Blake, and F. S. Rowland (2003), Seasonal variations of C_2-C_4 nonmethane hydrocarbons and C_1-C_4 alkyl nitrates at the Summit research station in Greenland, J. Geophys. Res., 108(D2) 4065, doi: 10.1029/2001JD001445.

Swarthout, R. F., R. S. Russo, Y. Zhou, A. H. Hart, and B. C. Sive (2013), Volatile organic compound distributions during the NACHTT campaign at the Boulder Atmospheric Observatory: Influence of urban and natural gas sources, J. Geophys. Res., 118, 10614–10637, doi: 10.1002/jgrd.50722.

Swarthout, R. F., R. S. Russo, Y. Zhou, B. M. Miller, B. Mitchell, E. Horsman, E. Lipsky, D. C. McCabe, E. Baum, and B. C Sive (2015), Impact of Marcellus Shale natural gas

development in Southwest Pennsylvania on volatile organic compound emissions and regional air quality, Environ. Sci. Technol., 49(5), 3175-3184, doi: 10.1021/es504315f.

Tackett, P. J., A. E. Cavender, A. D. Keil, P. B. Shepson, J. W. Bottenheim, S. Morin, J. Deary, A. Steffen, and C. Doerge (2007), A study of the vertical scale of halogen chemistry in the Arctic troposphere during Polar Sunrise at Barrow, Alaska, J. Geophys. Res., 112(D07306), doi: 10.1029/2006JD007785.

Thompson, C. R., P. B. Shepson, J. Liao, L. G. Huey, E. C. Apel, C. A. Cantrell, F. Flocke, J. Orlando, A. Fried, S. R. Hall, R. S. Hornbrook, D.J. Knapp, R. L. Mauldin III, D. D. Montzka, B. C. Sive, K. Ullmann, P. Weibring, and A. Weinheimer (2015), Interactions of bromine, chlorine, and iodine photochemistry during ozone depletions in Barrow, Alaska, *Atmos. Chem. Phys., 15,* 9651-9679, doi: 10.5194/acp-15-9651-2015.

Toyota, K., J. C. McConnell, R. M. Staebler, and A. P. Dastoor (2014), Air–snowpack exchange of bromine, ozone and mercury in the springtime Arctic simulated by the 1-D model PHANTAS – Part 1: In-snow bromine activation and its impact on ozone, Atmos. Chem. Phys., 14, 4101-4133, doi: 10.5194/acp-14-4101-2014.

U.S. EPA (United States Environmental Protection Agency) (2014a), Data from the Ambient Monitoring Archive for HAPs. Accessed 2014. http://www3.epa.gov/ttn/amtic/toxdat.html#data.

U.S. EPA (United States Environmental Protection Agency) (2014b), Data from the 2011 National Emissions Inventory, Version 1. Accessed 2014. http://www3.epa.gov/ttnchie1/net/2011inventory.html.

Villena, G., P. Wiesen, C. A. Cantrell, F. Flocke, A. Fried, S. R. Hall, R. S. Hornbrook, D. Knapp, E. Kosciuch, R. L. Mauldin III, J. A. McGrath, D. Montzka, D. Richter, K. Ullmann, J. Walega, P. Weibring, A. Weinheimer, R. M. Staebler, J. Liao, L. G. Huey, and J. Kleffmann (2011), Nitrous acid (HONO) during polar spring in Barrow, Alaska: A net source of OH radicals?, J. Geophys. Res., 116(D00R07), doi:10.1029/2011JD016643.

Volz-Thomas, A., J. Slemr, S. Konrad, Th. Schmitz, E. C. Apel, and V. A. Mohnen (2002), Quality assurance of hydrocarbon measurements for the German Tropospheric Research Focus (TFS), J. Atmos. Chem., 42, 255-279, doi: 10.1023/A:1015793319095.

Worton, D. R., W. T. Sturges, C. E. Reeves, M. J. Newland, S. A. Penkett, E. Atlas, V. Stroud, K. Johnson, N. Schmidbauer, S. Solberg, J. Schwander, and J.-M. Barnola (2012), Evidence from firn air for recent decreases in non-methane hydrocarbons and a 20th century increase in nitrogen oxides in the northern hemisphere, Atmos. Environ., 54, 592-602, doi: 10.1016/j.atmosenv.2012.02.084.

Wyngaard, J. C. (2010), Turbulence in the Atmosphere, New York: Cambridge University Press.

Yokouchi, Y., H. Akimoto, L. A. Barrie, J. W. Bottenheim, K. Anlauf, and B. T. Jobson (1994), Serial gas chromatographic/mass spectrometric measurements of some volatile organic compounds in the Arctic atmosphere during the 1992 Polar Sunrise Experiment, J. Geophys. Res., 99(D12), 25,379–25,389, doi: 10.1029/94JD00227.

Zhou, Y., H. Mao, R. S. Russo, D. R. Blake, O. W. Wingenter, K. B. Haase, J. L. Ambrose, R. K. Varner, R. Talbot, and B. C. Sive (2008), Bromoform and dibromomethane

measurements in the seacoast region of New Hampshire, 2002–2004, J. Geophys. Res., 113, D08305, doi: 10.1029/2007JD009103.

Table 1. Summary of volatile organic compounds observed using the Trace Organic Gas Analyzer (TOGA) during OASIS-2009

				All Tower Data			Clean-sector Tower Data			
VOC	LOD, pptv	Precision	Accuracy	Data Range (min - max), pptv	Mean ± 1σ Std. Dev., pptv	N[a]	Data Range (min - max), pptv	Mean ± 1σ Std. Dev., pptv	N[a]	Change during campaign, pptv day^{-1}
isobutane	3	± 3%	15%	30 - 7959	200 ± 200	3175	50 - 437	200 ± 100	2035	-6.0 ± 0.1
n-butane	3	± 3%	15%	25 - 17966	200 ± 400	3175	61 - 773	300 ± 200	2035	-10.7 ± 0.2
isopentane	3	± 3%	15%	4 - 10448	70 ± 200	2955	5 - 208	70 ± 50	1920	-3.01 ± 0.06
n-pentane	3	± 3%	15%	3 - 1960	50 ± 60	3170	8 - 222	50 ± 40	2106	-2.61 ± 0.05
benzene	25	± 5%	25%	37 - 879	100 ± 50	3041	37 - 196	100 ± 20	1981	-1.35 ± 0.02
toluene	1	± 3%	20%	3 - 11332	100 ± 500	3166	5 - 114	30 ± 20	2098	-1.60 ± 0.02
ethylbenzene + *m*-, *p*-xylene	1	± 3%	20%	bdl - 1413	10 ± 60	1915	bdl - 30	3 ± 4	1154	-0.179 ± 0.005
o-xylene	1	± 3%	20%	bdl - 347	3 ± 16	2966	bdl - 7	1 ± 1	555	-0.028 ± 0.001
sum of C_8-aromatics	1	± 3%	20%	bdl - 1761	20 ± 80	1915	bdl - 37	4 ± 4	1154	0.207 ± 0.006
acetaldehyde	3	± 5%	25%	bdl - 9120	100 ± 200	2842	bdl - 500	70 ± 50	2106	-0.92 ± 0.09
propanal	3	± 5%	25%	bdl - 527	20 ± 20	2677	bdl - 61	20 ± 10	2106	-0.64 ± 0.02
butanal	2	± 5%	25%	bdl - 241	10 ± 10	2905	bdl - 54	8 ± 7	1597	-0.28 ± 0.01
acetone	100	± 5%	25%	364 - 2210	900 ± 300	3175	364 - 1531	800 ± 300	2106	17.2 ± 0.2
MEK	3	± 5%	20%	59 - 334	190 ± 50	3065	59 - 296	190 ± 50	2103	1.30 ± 0.07
2-pentanone	3	± 5%	20%	3 - 315	20 ± 20	2634	3 - 45	20 ± 10	1753	-0.23 ± 0.01
methanol	50	± 5%	25%	229 - 6617	700 ± 500	3174	299 - 2589	600 ± 200	2035	5.0 ± 0.2
ethanol	3	± 5%	25%	9 - 9342	200 ± 400	2892	27 - 622	100 ± 50	1789	-1.39 ± 0.08

[a] Number of samples above limit of detection (LOD) and quantifiable in the chromatograms.

Table 2. Summary of selected volatile organic compounds observed in the canisters during OASIS-2009

				All Data			Clean-Sector Data		
VOC	LOD, pptv	Precision	Accuracy	Data Range (min - max), pptv	Mean ± 1σ Std. Dev., pptv	N	Data Range (min - max), pptv	Mean ± 1σ Std. Dev., pptv	N
ethane	3	1.1%	5%	1133 – 3412	2100 ± 400	92	1133 – 3230	2100 ± 400	54
ethyne	3	1.3%	5%	bdl – 1182	300 ± 200	86	bdl – 593	200 ± 200	51
propane	3	1.7%	5%	390 – 3129	900 ± 400	92	398 – 1881	800 ± 300	54
isobutane	3	1.3%	5%	30 – 5432	200 ± 600	92	58 – 403	140 ± 80	54
n-butane	3	1.4%	5%	34 – 9447	300 ± 1000	92	77 – 711	200 ± 100	54
isopentane	3	2.7%	5%	4 – 5261	200 ± 600	92	15 – 175	60 ± 40	54
n-pentane	3	3.4%	5%	6 – 1095	70 ± 100	92	13 – 232	50 ± 40	54

Table 3. Rate constants (cm^3 $molecule^{-1}$ s^{-1}) for the reactions of several species with OH radicals, Cl atoms and Br atoms at 248 K.

VOC	k_{OH} [a]	k_{Cl} [a]	k_{Br}
ethane	1.26×10^{-13}	5.55×10^{-11}	$< 10^{-19}$ [b]
propane	7.13×10^{-13}	1.40×10^{-10}	$< 10^{-17}$ [b]
isobutane	1.71×10^{-12}	1.40×10^{-10}	$<10^{-17}$ [b]
n-butane	1.72×10^{-12}	2.10×10^{-10}	$< 10^{-19}$ [b]
isopentane	3.06×10^{-12}	2.10×10^{-10}	-
n-pentane	2.93×10^{-12}	2.70×10^{-10}	-
ethyne	6.60×10^{-13}	7.34×10^{-11}	3.74×10^{-14} [c]
acetaldehyde	1.67×10^{-11}	8.00×10^{-11}	2.82×10^{-12} [c]
propanal	2.46×10^{-11}	1.74×10^{-10}	4.91×10^{-12} [d]
butanal	3.13×10^{-11}	2.30×10^{-10}	6.52×10^{-12} [d]
acetone	1.37×10^{-13}	1.29×10^{-12}	-
MEK	9.97×10^{-13}	4.00×10^{-11}	-
O_3	-	1.02×10^{-11}	6.76×10^{-13} [e]

[a] *Calvert et al*., [2015].
[b] NIST Chemical database, http://kinetics.nist.gov/kinetics/index.jsp.
[c] *Atkinson et al*., [2006].
[d] *Ramacher et al*., [2000].
[e] *Atkinson et al*., [2007].

Table 4. Summary of correlations between clean-sector VOCs observed by TOGA and in the canisters

	linear least-squares fit			ODR fit[a]	
TOGA VOCs	slope[a]	intercept[a]	r^2	slope	intercept
acetone vs. MEK	3.74 ± 0.09	140 ± 20	0.438	8.4 ± 0.2	-750 ± 40
acetone vs. 2-pentanone	-	-	0.034	-	-
MEK vs. 2-pentanone	-	-	0.208	-	-
acetaldehyde vs. acetone	-	-	0.146	-	-
acetaldehyde vs. propanal	2.14 ± 0.06	42 ± 2	0.414	4.9 ± 0.1	-12 ± 3
acetaldehyde vs. butanal	4.7 ± 0.1	38 ± 2	0.455	10.3 ± 0.3	-18 ± 3
propanal vs. butanal	1.87 ± 0.02	1.2 ± 0.3	0.770	2.32 ± 0.03	-3.3 ± 0.4
methanol vs. ethanol	-	-	0.054	-	-
methanol vs. acetone	-	-	0.187	-	-
MEK vs. *n*-butane	-	-	0.062	-	-
isobutane vs. *n*-butane	0.549 ± 0.001	25.3 ± 0.3	0.993	0.550 ± 0.001	25.0 ± 0.3
isopentane vs. *n*-pentane	1.059 ± 0.004	5.2 ± 0.3	0.975	1.073 ± 0.003	4.4 ± 0.3
n-butane vs. *n*-pentane	3.255 ± 0.009	37.9 ± 0.8	0.985	3.302 ± 0.009	34.8 ± 0.8
n-butane vs. benzene	7.23 ± 0.09	-486 ± 9	0.774	9.3 ± 0.1	-700 ± 10
n-butane vs. toluene	6.64 ± 0.06	40 ± 3	0.842	7.86 ± 0.08	1 ± 3
benzene vs. toluene	0.793 ± 0.008	76.9 ± 0.3	0.817	0.865 ± 0.009	76.6 ± 0.4
toluene vs. C_8 aromatics	3.08 ± 0.07	28.4 ± 0.6	0.603	5.0 ± 0.1	16.4 ± 0.9
Canister VOCs					
ethane vs. propane	1.02 ± 0.06	1300 ± 50	0.858	1.11 ± 0.06	1230 ± 50
n-butane vs. propane	0.410 ± 0.008	-109 ± 7	0.978	0.411 ± 0.009	-110 ± 7
n-pentane vs. propane[b]	0.107 ± 0.003	-37 ± 9	0.967	0.107 ± 0.003	-38 ± 2
isobutane vs. *n*-butane	0.549 ± 0.008	20 ± 2	0.989	0.551 ± 0.008	20 ± 2
isopentane vs. *n*-pentane[b]	0.99 ± 0.03	8 ± 2	0.965	1.01 ± 0.03	7 ± 2
n-butane vs. *n*-pentane[b]	3.79 ± 0.07	40 ± 4	0.981	3.86 ± 0.07	36 ± 4

[a] Where the coefficient of determination $r^2 > 0.4$ (correlation coefficient $r > 0.633$).

[b] With data from 19 March at 15:00 AKST with *n*-pentane = 232.4 pptv omitted.

Table 5. A comparison of concentrations and production/loss rates during the OASIS-2009 study

	Time Period		
Parameter	7-15 March	1-14 April	As noted
[OH], molecules cm^{-3}	3.2×10^5	4.5×10^5	
[Cl][a], atoms cm^{-3}	3.0×10^3	3.0×10^3	
$[Cl]_{SS}$[b], atoms cm^{-3}			3.4×10^4
Midday $[Br]_{SS}$[c], atoms cm^{-3}			1.0×10^9
[ethane], pptv	2500	1900	
[propane], pptv	1300	500	
[isobutane], pptv	275	100	
[*n*-butane], pptv	400	170	
[isopentane], pptv	115	50	
[acetone], pptv	500	1000	
[MEK], pptv	180	230	
J(acetaldehyde), s^{-1}	1.4×10^{-7}	6.1×10^{-7}	
J(acetone), s^{-1}	3.5×10^{-9}	2.2×10^{-8}	
J(MEK), s^{-1}	2.4×10^{-7}	9.3×10^{-7}	
Calculated propane loss rate			
OH chemistry only, pptv h^{-1}	1.1	0.58	
OH and Cl chemistry, pptv h^{-1}	3.0	1.3	
OH and $[Cl]_{SS}$[b] chemistry, pptv h^{-1}			23.5
Observed propane loss rate[d], pptv h^{-1}			1.0 ± 0.2
Calculated acetone formation rate			
OH chemistry only, pptv h^{-1}	1.4	0.53	
OH and Cl chemistry, pptv h^{-1}	2.9	1.1	
OH and $[Cl]_{SS}$[b] chemistry, pptv h^{-1}			18.2
Observed acetone formation rate[d], pptv h^{-1}			0.72 ± 0.01
Calculated MEK formation rate			
OH chemistry only, pptv h^{-1}	0.40	-0.80	
Observed MEK formation rate[d], pptv h^{-1}			0.054 ± 0.003
Calculated acetaldehyde formation rate			
OH chemistry only, pptv h^{-1}	-1.8	-2.1	
OH and $[Cl]_{SS}$[b] chemistry, pptv h^{-1}			11
OH, $[Cl]_{SS}$[b] and $[Br]_{SS}$[c], pptv h^{-1}			< -100

[a] Estimated "moderate" Cl-atom concentration.
[b] Calculated steady state Cl-atom concentration at measurement site for 17-29 March.
[c] Calculated midday steady state Br-atom concentration during ODE 3: 26-29 March.
[d] Calculated using overall campaign changes in concentration.

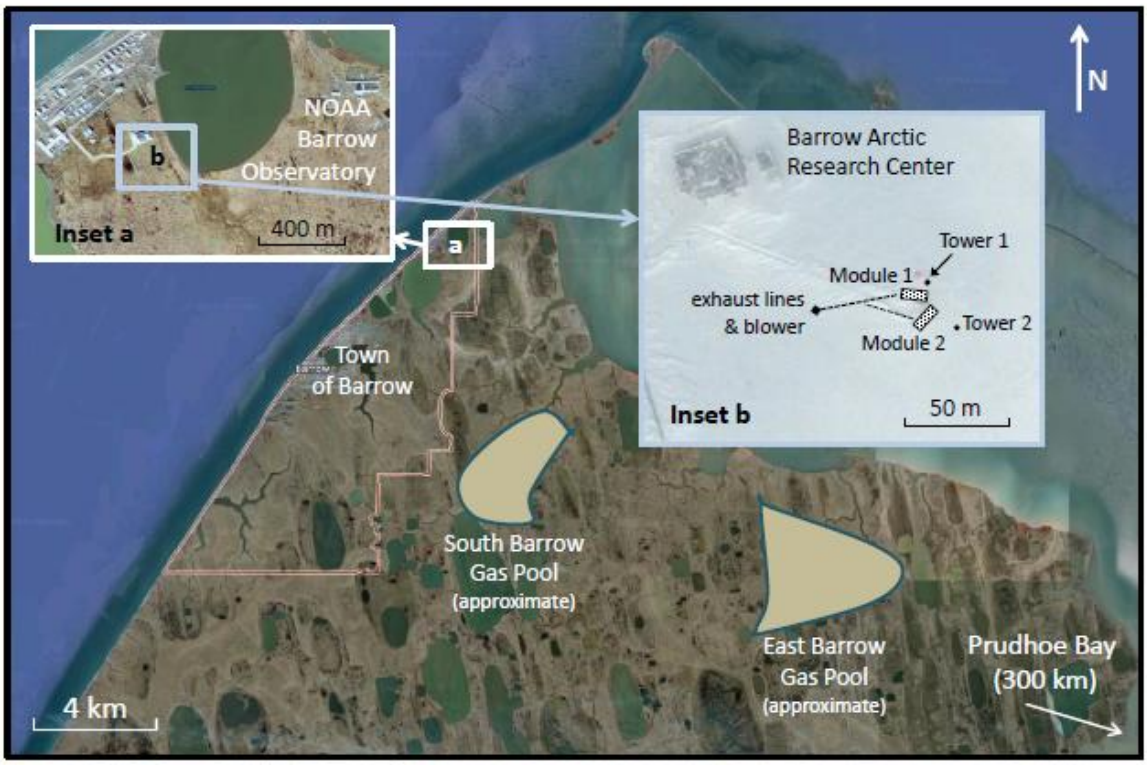

Figure 1. Map of Barrow region showing the proximity of the OASIS-2009 field site to the Town of Barrow, Regional Natural Gas Pools, and Prudhoe Bay region. Inset (a) shows the location of the field site relative to the NOAA Barrow Observatory. Inset (b) shows a schematic of the field site during the project, including the snow path from the Barrow Arctic Research Center to the modules.

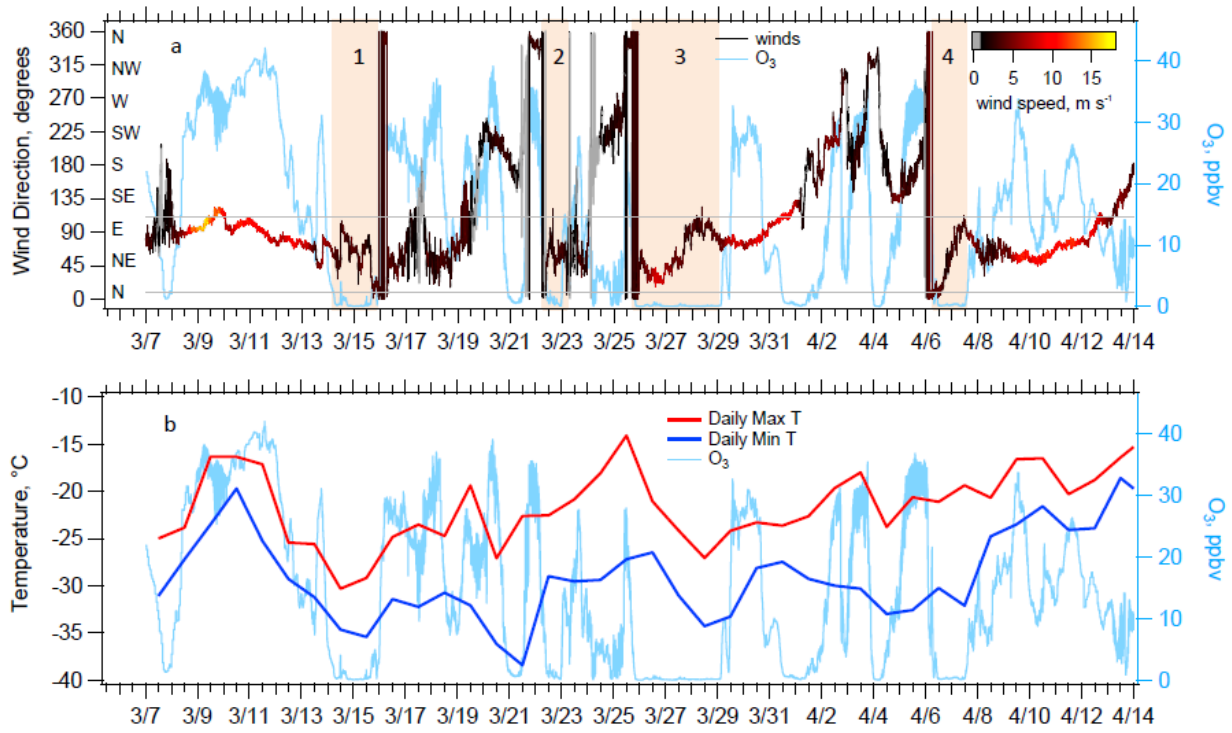

Figure 2. (a) Time series of wind directions and O_3 observations between 7 March and 14 April 2009. Wind data are colored according to the color scale on the plot, with wind speeds below 1 m s^{-1} (i.e., calm) colored light grey. Data within the grey boundaries at 10° and 110° are considered as originating from the clean sector. Four ozone depletion events (ODEs) in which winds primarily originated from the clean sector are highlighted and numbered 1 through 4. (b) Daily maximum and minimum temperatures with the 1-min ozone trace superimposed in the background.

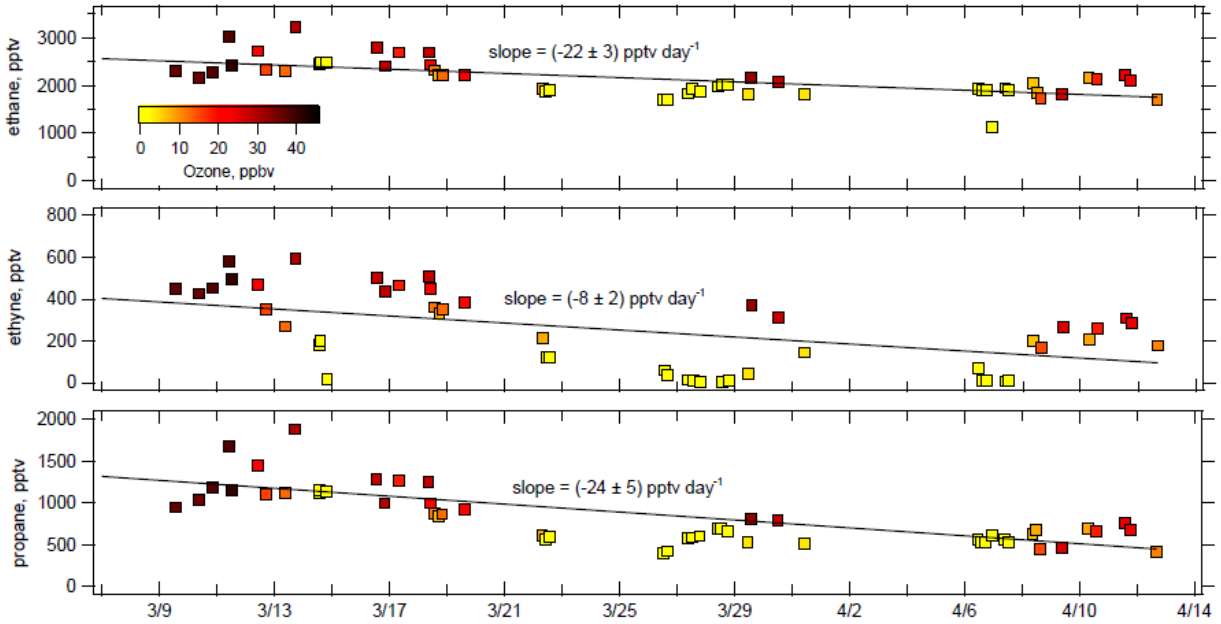

Figure 3. Time series of clean-sector canister ethane, ethyne and propane mixing ratios, colored by observed ozone mixing ratios. Also shown are campaign average linear fits to the data, with the slope in pptv day^{-1} indicated on each plot.

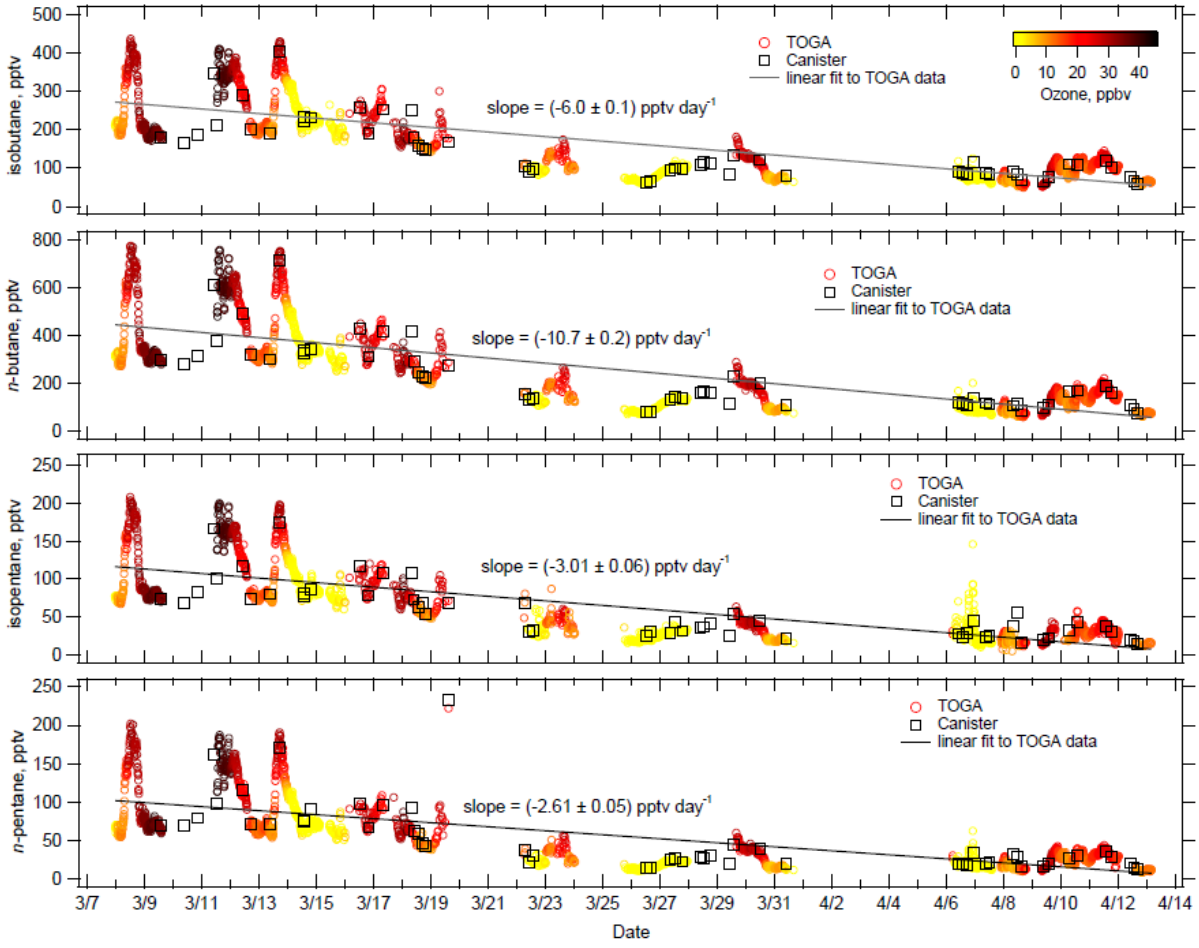

Figure 4. Time series of clean-sector TOGA and canister isobutane, *n*-butane, isopentane and *n*-pentane mixing ratios, with the TOGA data colored by observed ozone mixing ratios. Also shown are campaign average linear fits to the TOGA data, with the slope in pptv day^{-1} indicated on each plot.

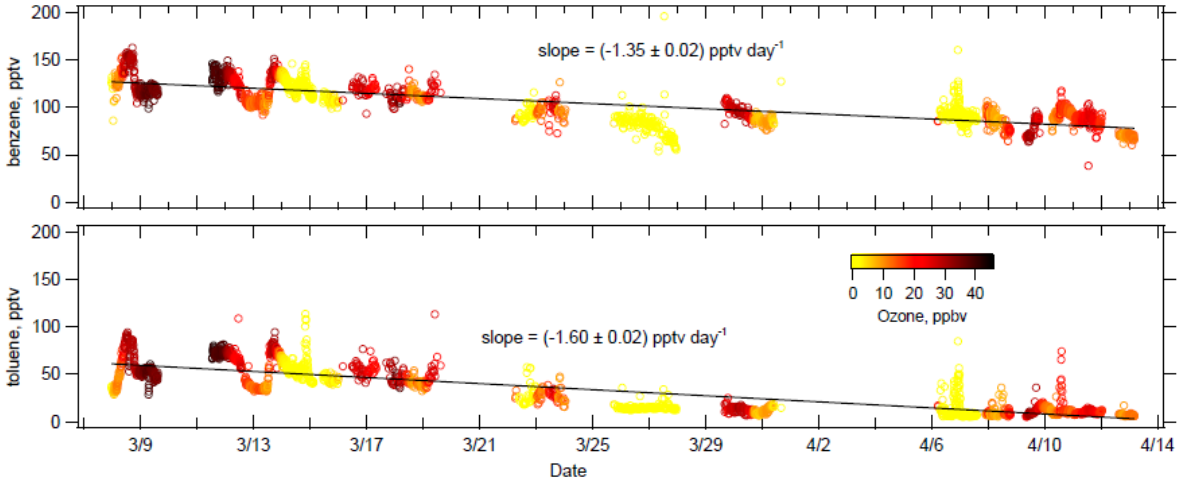

Figure 5. Time series of clean-sector benzene and toluene mixing ratios, as in Figure 4.

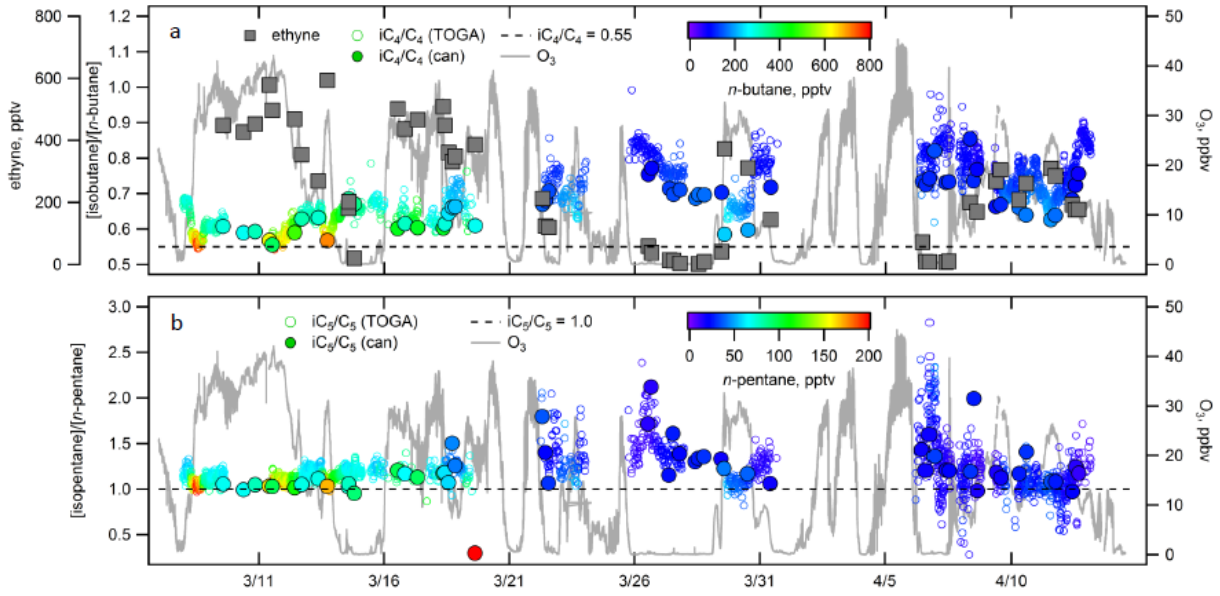

Figure 6. Time series of (a) isobutane/*n*-butane (iC_4/C_4) ratios colored by *n*-butane mixing ratios and (b) isopentane/*n*-pentane (iC_5/C_5) ratios colored by *n*-pentane mixing ratios. O_3 mixing ratios are shown on both plots. Included on (a) are the observed ethyne mixing ratios. For comparison, estimated regional oil and gas emission ratios $iC_4/C_4 = 0.55$ and $iC_5/C_5 = 1.0$ are shown on (a) and (b), respectively.

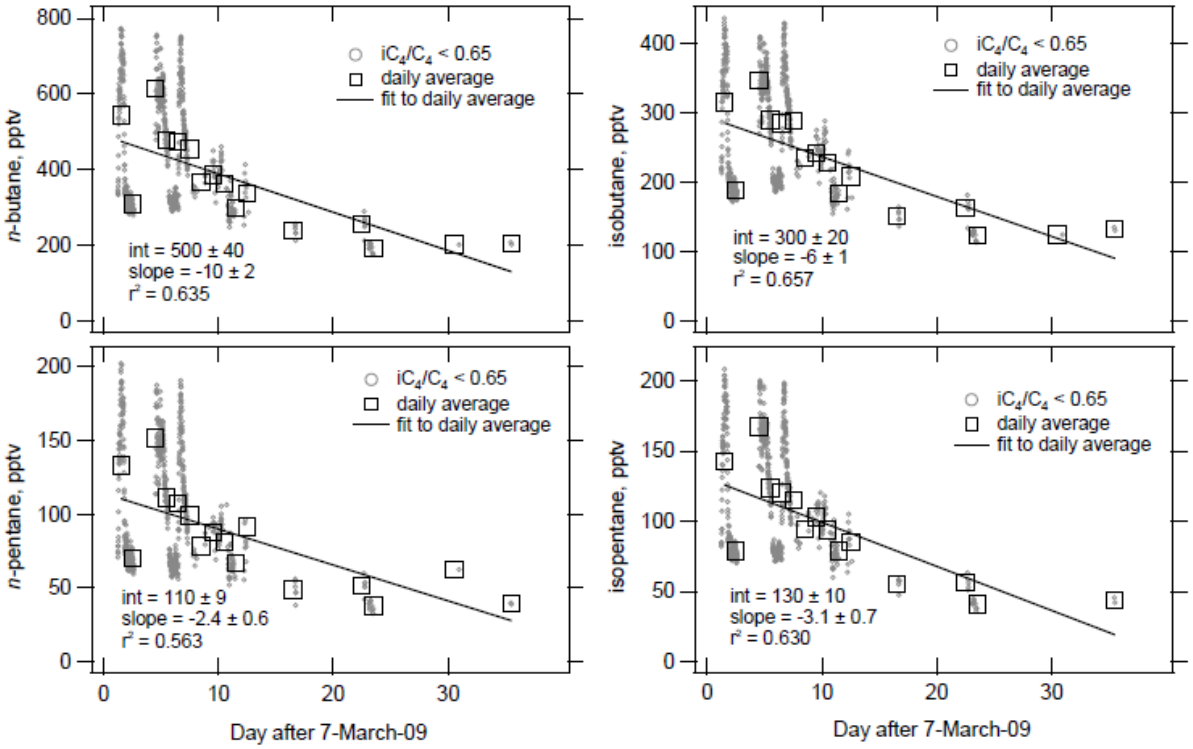

Figure 7. Time series of the TOGA-observed mixing ratios for C_4 and C_5 NMHC. Small grey circles are all the clean-sector data when $iC_4/C_4 < 0.65$, suggesting little impact from chlorine chemistry, and open squares are the daily averages of the above data. Linear least-squares fits to the daily averages with intercept, r^2 value and slope used to estimate $[RH]_{bkg,t}$ are shown on each plot.

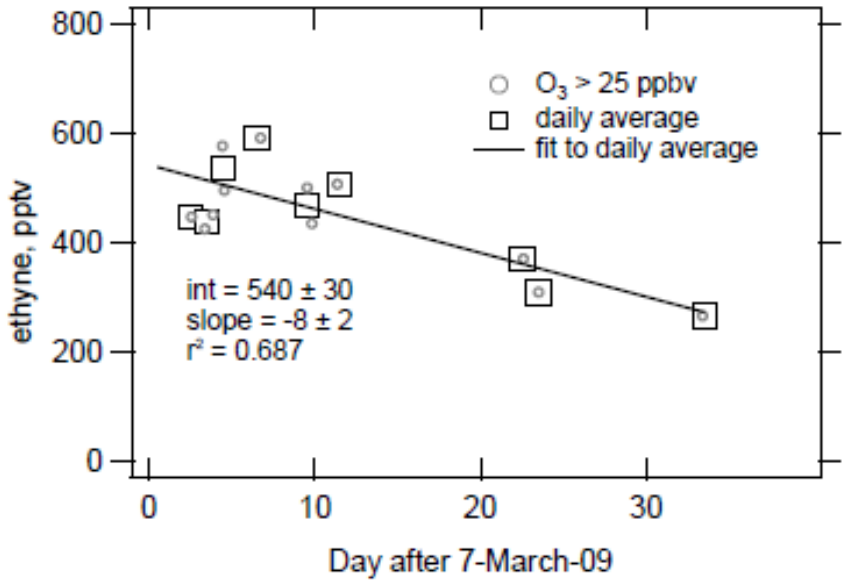

Figure 8. Time series of the ethyne mixing ratios. Small grey circles are all clean-sector data during times when O_3 > 25 ppbv, indicating little impact of bromine chemistry, and open squares are the daily averages of the above data. A linear fit to the daily averages with intercept, r^2 value and slope used to estimate $[C_2H_2]_{bkg,t}$ is shown.

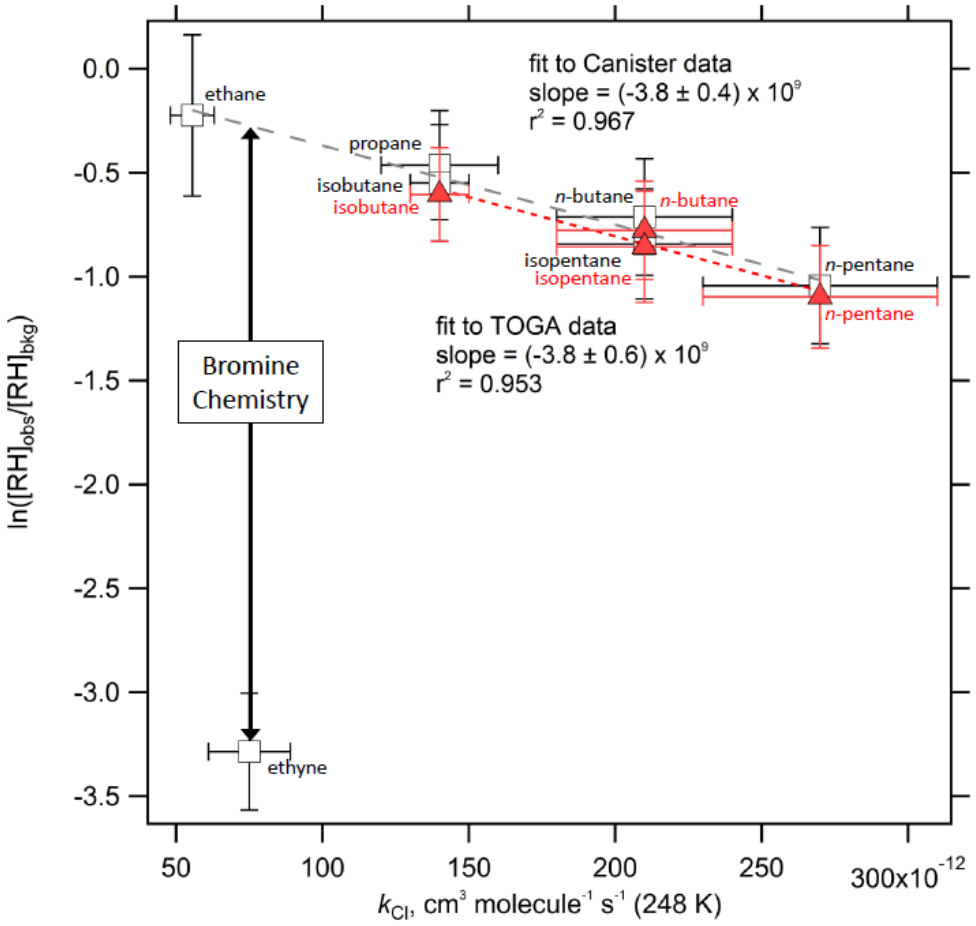

Figure 9. Correlation between the ratio of observed hydrocarbon concentrations and calculated background hydrocarbon levels against Cl-atom rate coefficients for TOGA (red triangles; red text labels) and canister data (open squares; black text labels) from 27 March between 08:56 and 09:00 AKST. Separate linear least-squares fits to the TOGA (red dotted) alkane and canister (grey dashed) data are shown. The impact of Br-atom chemistry can be seen in the difference between the fit to the canister alkane data and the ethyne data point. Error bars show the uncertainties in the Cl-atom rate coefficients (X-axis) and the uncertainties in the natural logarithm of the ratio (Y-axis) propagated from the uncertainties in the measurements $[RH]_{obs}$ (± 10%) and in the $[RH]_{bkg,t}$ values from the linear fits shown in Figures 7, 8, and S2.

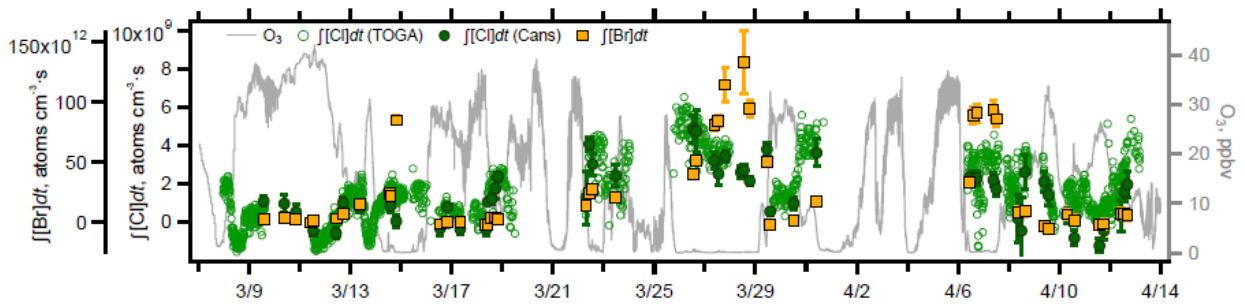

Figure 10. Time series of the calculated integrated halogen atom concentrations, ∫[Br]*dt* and ∫[Cl]*dt*, and the locally-observed O_3 mixing ratios. Error bars for the canister-derived ∫[Cl]*dt* and ∫[Br]*dt* are as described in the text.

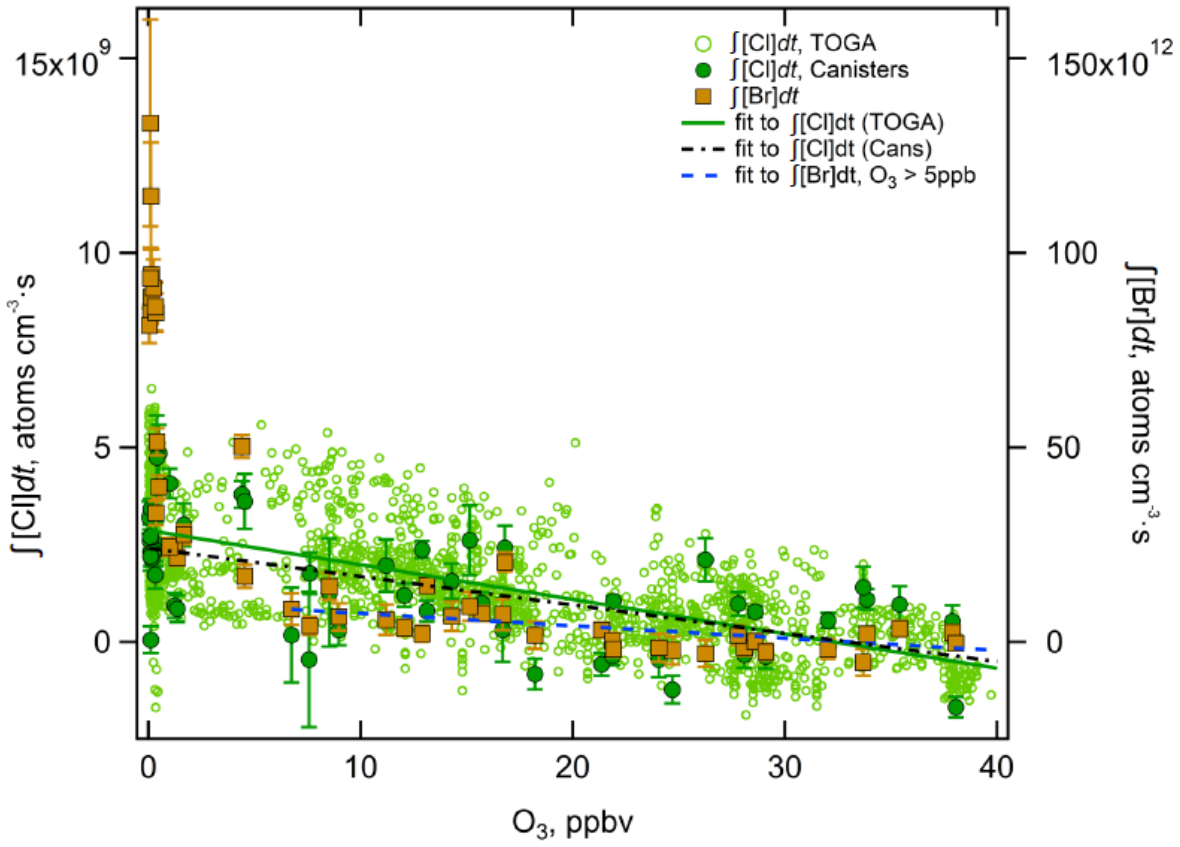

Figure 11. Plot of the O_3 dependence of the calculated integrated halogen atom concentrations, ∫[Br]*dt* and TOGA- and canister-derived ∫[Cl]*dt*. Linear least-squares fits to all the TOGA-derived (solid green line) and canister-derived ∫[Cl]*dt* data (dashed black line), and to the ∫[Br]*dt* data for O_3 > 5 ppbv (dashed blue line) are shown. Details for all fits are given in the text.

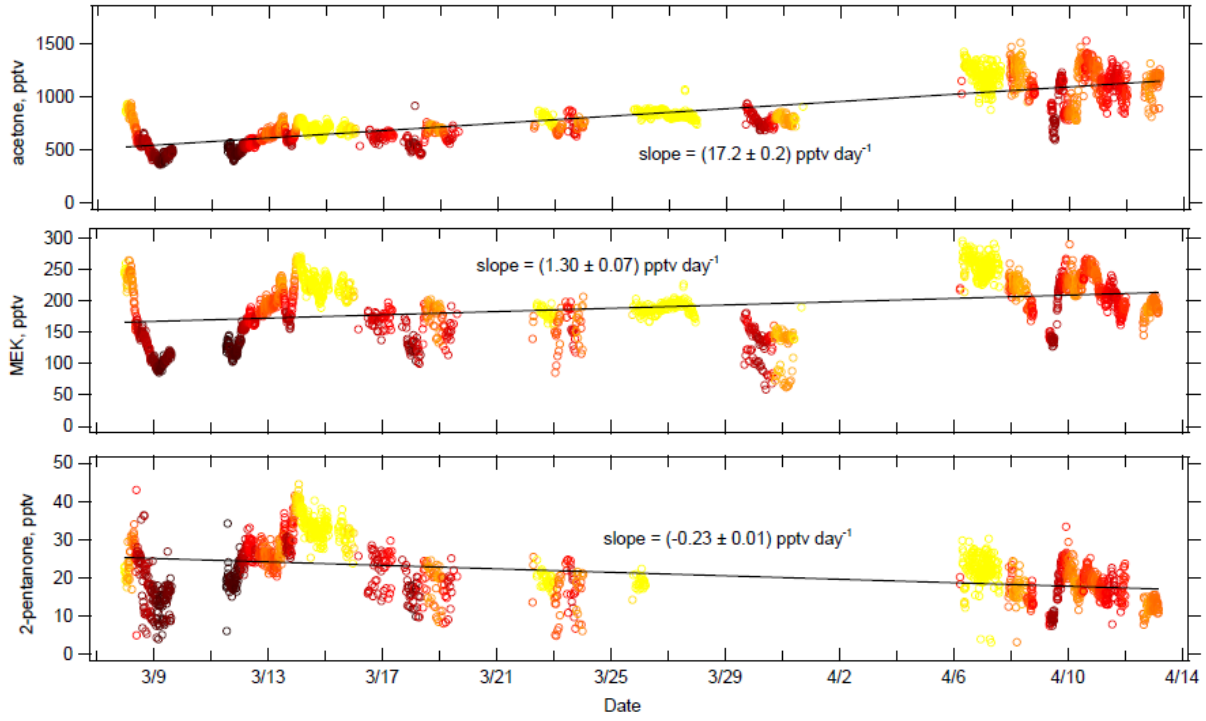

Figure 12. Time series of the observed clean-sector mixing ratios for acetone, MEK and 2-pentanone, as in Figures 4 and 5.

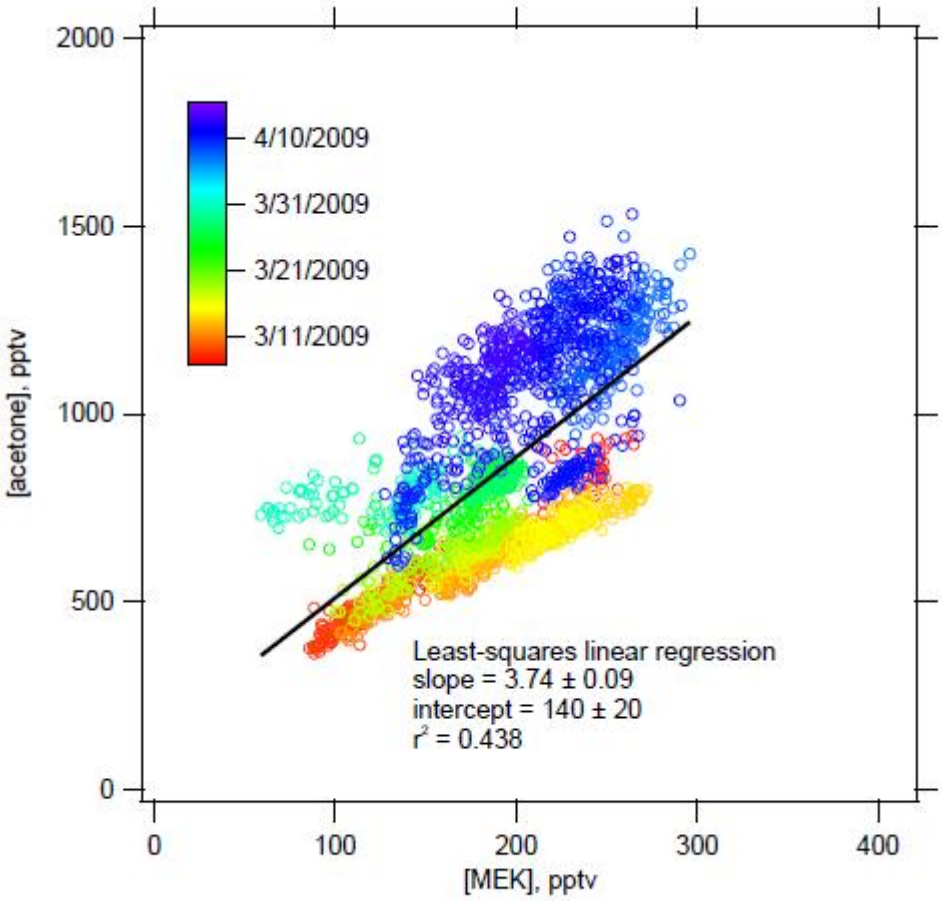

Figure 13. Correlation plot of clean-sector acetone and MEK observations colored by sample date. A linear least-squares fit to the data is shown.

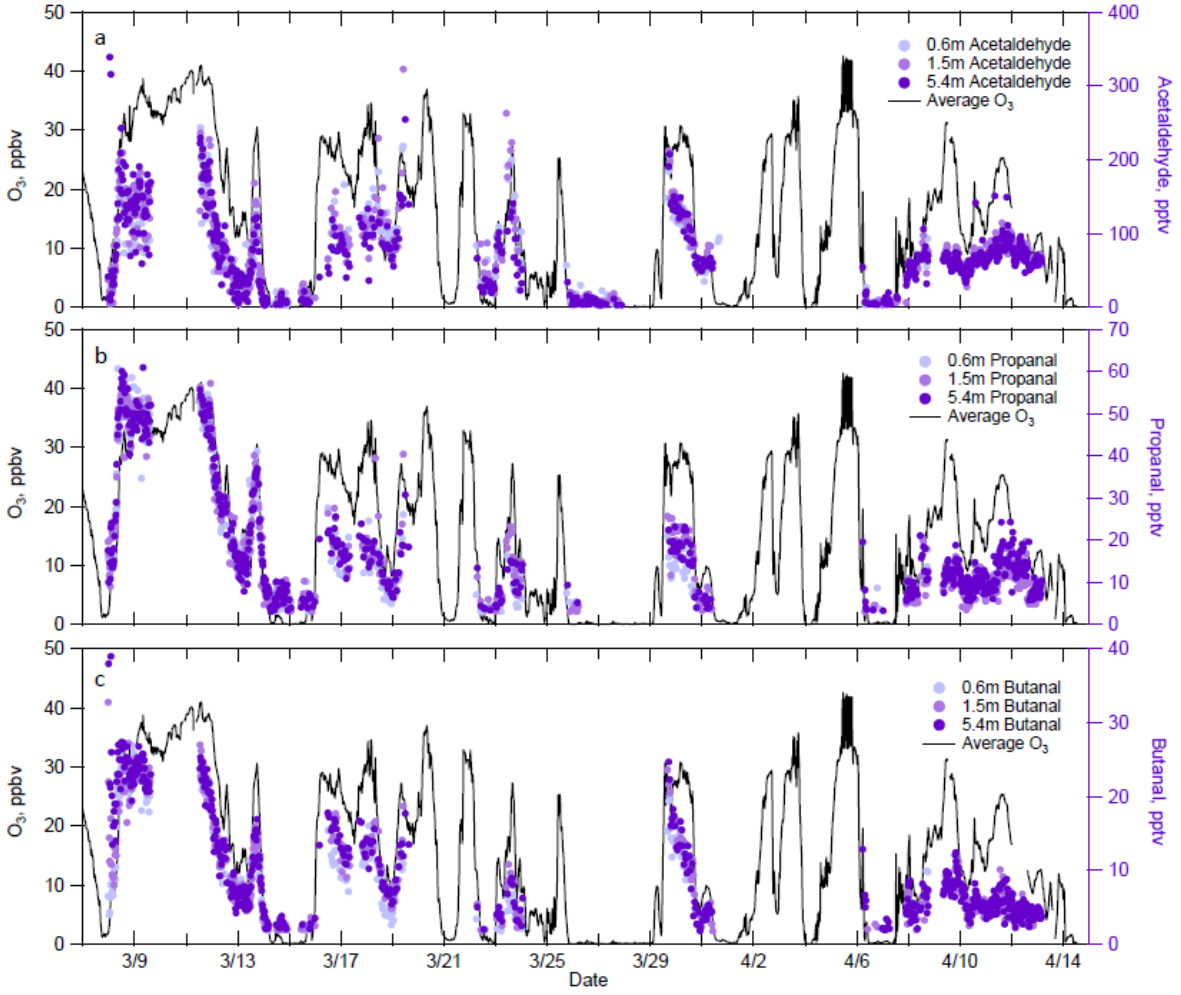

Figure 14. Time series of average ozone mixing ratios and altitude-dependent clean-sector aldehyde mixing ratios.